

**ACOUSTIC EMISSION MONITORING OF THE POWDER  
BED FUSION PROCESS WITH MACHINE LEARNING  
APPROACH**

Acoustic Emission Monitoring of the Powder Bed Fusion Process with Machine learning  
Approach

By

Mohammad Ghayoomi Mohammadi, BSc.

A Thesis

Submitted to the School of Graduate Studies in Partial Fulfillment of the Requirements  
for the Degree Master of Applied Science

McMaster University

© Copyright by Mohammad Ghayoomi, September 2021

# Master of Applied Science (2021)

## (Mechanical Engineering)

McMaster University  
Hamilton, Ontario

**TITLE:** Acoustic Emission Monitoring of the Powder Bed Fusion Process with Machine learning Approach

AUTHOR: Mohammad Ghayoomi Mohammadi  
B.Sc. in Mechanical Engineering (Amirkabir University of Technology (Tehran Polytechnic))

SUPERVISORS: Dr. M. A. Elbestawi

NUMBER OF PAGES: xi, 98

## Abstract

Laser powder bed fusion (L-PBF) is an additive manufacturing process where a heat source (such as a laser) consolidates material in powder form to build three-dimensional parts. For quality control purposes, this thesis uses real-time monitoring in L-PBF. Defects such as pores and cracks can be detected using Acoustic Emission (AE) during the powder bed selective laser melting process via the machine learning approach. This thesis investigates the performance of several Machine Learning (ML) techniques for online defect detection within the Laser Powder Bed Fusion (L-PBF) process. The goal is to improve the consistency in product quality and process reliability. The application of acoustic emission (AE) sensors to receive elastic waves during the printing process is a cost-effective way of meeting such a goal.

For the first step, stainless steel 316L was produced via eight parameters. The acoustic emission signals received during the printing and data collection steps are analyzed using an AE sensor under various process parameters. Several time and frequency-domain features were extracted from data during the mining process from the AE signals.

K-means clustering is employed during unsupervised learning, and a neural network approach was used for the supervised machine learning on the dataset. Data labelling is conducted for different laser powers, clustering results, and signal

time durations. The results showed the potential of real-time quality monitoring using AE in the L-PBF process.

Some process parameters within this project were intentionally adjusted to create three various levels of defects in H13 tool steel samples. First classes were printed with minimum defects, second classes with intentional cracks, and last classes with intentional cracks and porosities. AE signals were acquired during the samples' manufacturing process. Three different machine learning (ML) techniques were applied to analyze and interpret the data. First, using a hierarchical K-means clustering method, the data was labelled. This was followed by a supervised deep learning neural network (DL) to match acoustic signals with defect type. Second, a principal component analysis (PCA) was used to reduce the dimensionality of the data. A Gaussian Mixture Model (GMM) enabled the fast detection of defects, which is suitable for online monitoring. Third, a variational auto-encoder (VAE) approach was used to obtain a general feature of the signal, which could be used as an input for the classifier. Quality trends in AE signals collected from 316L samples were successfully detected using a supervised DL trained on the H13 tool steel dataset. The VAE approach shows a new method for detecting defects within the L-PBF processes, which would eliminate the need for model training in different materials.

## Preface

This thesis project deals with the Monitoring of the LPBF process by Acoustic emission with machine learning methods. It is composed of two journal papers listed as followed, based on the publication order:

Chapter 2: A version of this chapter is published as a research paper: Mohammadi, M. G., & Elbestawi, M. (2020). Real Time Monitoring in L-PBF Using a Machine Learning Approach. *Procedia Manufacturing*, 51, 725-731.

Chapter 3: A version of this chapter is published as a research paper: Mohammadi, M. G., Mahmoud, D., & Elbestawi, M. (2021). On the application of machine learning for defect detection in L-PBF additive manufacturing. *Optics & Laser Technology*, 143, 107338.

*To my parents and my sister*

*I owe you everything.*

## Acknowledgements

First, I would like to convey my most sincere gratitude to my supervisor Dr. Mohamed Elbestawi who has been a tremendous mentor and teacher. I would like to thank you for your support and patience along the way in this journey. Your guidance has been and will be an invaluable asset in my academic life.

I would like to show my appreciation to my colleagues in the AMG group at McMaster University for the discussions, presentation rehearsals, and fruitful group meetings.

# Contents

	Page
<b>Abstract .....</b>	<b>i</b>
<b>Preface .....</b>	<b>iii</b>
<b>Acknowledgements .....</b>	<b>v</b>
<b>Contents .....</b>	<b>vi</b>
<b>List of Figures .....</b>	<b>ix</b>
<b>List of Tables .....</b>	<b>xi</b>
1    Introduction.....	1
1.1    Motivation.....	3
1.2    Schematic model for online quality control of the L-PBF process .....	4
1.3    Schematic AE setup for monitoring the L-PBF process.....	5
1.4    Research objectives.....	6
1.5    Thesis outline.....	7
1.6    References.....	9
2    Literature review.....	10
2.1    Background .....	11
2.2    Potentials and challenges.....	22
2.3    Standardization requirements in ML .....	26
2.4    Summary.....	27
2.5    References.....	29
3    Real Time Monitoring in L-PBF Using a Machine Learning Approach .....	32

<b>3.1</b>	<b>Introduction.....</b>	<b>34</b>
<b>3.2</b>	<b>Experimental procedures .....</b>	<b>37</b>
3.2.1	Feedstock materials .....	37
3.2.2	Selective laser melting processing.....	37
3.2.3	AE system.....	38
3.2.4	K-Means Clustering algorithm[8] .....	39
3.2.5	Deep learning for classification.....	40
<b>3.3</b>	<b>Results .....</b>	<b>43</b>
3.3.1	Time-domain data responses for the whole printing process .....	43
3.3.2	Unsupervised results.....	47
3.3.3	Supervised results.....	51
<b>3.4</b>	<b>Conclusion .....</b>	<b>52</b>
<b>3.5</b>	<b>References.....</b>	<b>53</b>
4	On the application of machine learning for defect detection in L-PBF additive manufacturing .....	54
<b>4.1</b>	<b>Introduction.....</b>	<b>57</b>
<b>4.2</b>	<b>Theoretical background .....</b>	<b>61</b>
4.2.1	AE Signal Processing .....	61
4.2.1.1	Fast Fourier Transform.....	61
4.2.1.2	Discrete Cosine Transform (DCT).....	62
4.2.2	Machine learning algorithms:.....	63
4.2.2.1	K-Means Clustering Algorithm.....	63
4.2.2.2	PCA- GMM.....	64
4.2.2.3	Variational Auto Encoders (VAE) .....	67

4.2.2.3.1 Encoder (Inference) Network: .....	68
4.2.2.3.2 Decoder (Generative) Network: .....	68
4.2.2.3.3 Re-parameterization: .....	68
4.2.2.3.4 Loss function: .....	68
4.2.2.4 Deep learning for classification (DL).....	69
<b>4.3 Experimental setup:.....</b>	<b>71</b>
4.3.1 L-PBF processing .....	71
4.3.2 AE system.....	74
<b>4.4 Results and discussion: .....</b>	<b>76</b>
4.4.1 K-Means Hierarchical Clustering for labeling .....	76
4.4.2 Deep Learning Classifier .....	80
4.4.3 PCA-GMM .....	82
4.4.4 VAE.....	84
4.4.5 Generalization of the classifiers .....	87
<b>4.5 Conclusion: .....</b>	<b>90</b>
<b>4.6 References:.....</b>	<b>91</b>
 5 Summary and Conclusions .....	94
5.1 Summary and conclusive remarks .....	95
5.2 Strength, limitations, and future work.....	96
5.3 Contribution .....	98

## List of Figures

Figure 1.1Flow chart for the online quality control of the L-PBF process.....	4
Figure 1.2 schematic of AE setup for monitoring L-PBF process.....	5
Figure 1.3 Structure of the thesis .....	8
Figure 3.1. Printed parts on the build plate.....	37
Figure 3.2Schematic of layers. networks, loss function, and optimizer in a deep learning model .....	41
Figure 3.3(a) Loss value and (b) accuracy in each epoch in the training part .....	42
Figure 3.4Time-domain AE signal feature .....	45
Figure 3.5(a) Rise time (b) Energy (c) Counts Vs Time for the whole process.....	46
Figure 3.6. Schematic illustrations of the path that waves travel to reach the AE sensor in the case of (a) first layer, and (b) multiple layers. ....	47
Figure 3.7Cluster results in the frequency domain .....	49
Figure 3.8Microstructures of the top surfaces of samples with (a) low-quality (b) medium-quality and (c) high quality .....	50
Figure 4.1VAE architecture with more details illustrated [35].....	67
Figure 4.2. The process chamber showing the cylindrical samples printed on the build plate .....	72
Figure 4.3: The cross-section of the samples along the build height with (a) no defects (class 1), (b) cracks only (class 2), and (c) both cracks and porosities (class 3).....	77
Figure 4.4: Schematic of the Hierarchal K-Means method.....	79
Figure 4.5: Frequency spectrum of H13 samples with intentional defects (a) minimum defects (class 1), (b) cracks only (class 2), and (c) porosities (class 3). .....	82
Figure 4.6The reduced data to 2D along with the fit gaussian model.....	83
Figure 4.7Waveform of example data chosen for anomaly detection validation.....	84

Figure 4.8: The architecture of the combined model ..... 85

Figure 4.9: a) The loss value and b) the mean squared error versus the number of epochs  
for the training and test step errors when the learning rate is 0.0020. ..... 86

Figure 4.10 The original and reconstructed signal obtained by the proposed VAE structure,  
a) original signal (encoder input) and b) reconstructed signal (decoder's output). ..... 87

## List of Tables

Table 3-1laser power and energy density of each test sample.....	38
Table 3-2AE system filtering parameters.....	39
Table 3-3Details of layers, networks in the deep learning model.....	41
Table 3-4Time-domain AE signal features with their definition.....	44
Table 3-5. Confusion Matrix.....	51
Table 4-1: Parameters for H13 Tools Steel test experiments.....	72
Table 4-2: Different defect classes used for labelling the classifiers.....	73
Table 4-3: Parameters for stainless steel 316L test experiments .....	74
Table 4-4: The confusion Matrix of using DL model.....	81
Table 4-5: Performance parameters used to classify the defect types. ....	81
Table 4-6: Percentage of defect detection on 316L test dataset by classifier 1. ....	88
Table 4-7: Percentage of defect detection on 316L test dataset by classifier 2. ....	89

## Introduction

A sub-field of Additive Manufacturing(AM), known as Laser Powder Bed Fusion (L-PBF), uses powder as the raw material, along with a heat source (laser) to fabricate the desired part. Owing to its unique capabilities, L-PBF has attracted the attention of different industrial sectors. The building platform is then heated if required and using a recoater, the first layer of powder is spread on the building platform. The recoater used could have a blade or a roller form. The laser begins scanning specific locations on the powder bed according to the part's geometry. The powder gains energy and transforms from a solid to a liquid state. The layer is subjected to the atmosphere and cools down very rapidly, solidifying into the first layer. The build platform is moved one layer downwards, while the powder dispenser is moved one layer upwards. The recoater spreads a fresh layer of powder on the previously solidified layer, and this process repeats until the whole part is manufactured, layer by layer.

A good method for understanding the numerous L-PBF process parameters is to categorize them according to time increments in which these parameters can be measured, whether they be controlled or chosen[1]. These classifications can be pre-process, in-process, or post-process. Pre-process parameters may be related to the material, for example, related to powder type, size, shape, or distribution. The parameters may also be related to the machine, such as laser type, mode, spot size, and laser scanning method. They could also be related to the building chamber, such as to the type of inert gas, build plate temperature, and inert gas pressure. Post-process parameters are typically related to part's performances in terms of mechanical properties. The focus of this paper

is on the in-process parameters, such as laser power, scan speed, scanning strategy, and layer thickness.

The defects generated in the parts manufactured via the L-PBF process can be classified into three categories; defects from machine parameters, from setup, or ones due to damage in the equipment or miscalibration [2]. The adjustment of laser power, scan speed, or hatch spacing can result in porosities, which can further be classified into lack of fusion or keyhole defects. The second category of defects is related to inadequate support placements or failures in applying a design for additive manufacturing approach while parts are being designed. These defects may lead to uneven powder spreading or high thermal gradients, which can lead to residual stresses and formation of cracks.

The third category of defects is related to faults and errors which might occur during the printing process. The levelling of the build plate and its orientation or alignment to a recoater could create an uneven powder layer, which would lead to a failure in some parts of the build plate. Powder particles that have adhered to the recoater may be plowed across the new powder layer, leading to a non-uniform powder layer. The recoater blade could also impact warped parts or edges, causing them to be removed from the build plate and hit other components.

The laser interacts with the powder being melted during the L-PBF process. This laser is either absorbed, reflected, refracted, scattered, or transmitted. It is expected that heating, melting, vaporization, or forming plasma might occur [3]. These phenomena present the opportunity to

monitor the process using a variety of methods, like monitoring the radiation, the acoustic, the acoustic emission, or the electromagnetic emission.

## 1.1 Motivation

It is of great importance to use the machine learning approach, presenting a novel Acoustic Emission-based approach with the aim of examining the real-time monitoring of L-PBF. Using the machine learning method, the present study aims to detect a variety of defects like pores and cracks during the power bed selective laser melting process. Moreover, through the use of Fast Fourier Transform (FFT), the frequency-time domain was obtained, which included pure consolidation, micro-cracks, and porosity. Nowadays, the importance and practicality of L-PBF in the industry are visible, and the benefits of ML in this technology are remarkable.

It is worth mentioning that making a comparison between the performance of several machine learning methods for an online monitoring system in the L-PBF process can bring considerable and important results. In addition, making this comparison with the aim of enhancing the product quality and making the L-PBF a reliable technique in terms of accuracy, time, and authenticity is of great significance. A hierarchical K-Means clustering method, PCA-GMM technique, and VAE method were examined in detail. The main focus of this study is optimizing the ML methods' practicalities for online monitoring of the L-PBF process, which can lead to acceptable and striking results. The results of this study are very advantageous in both industries and in terms of practical processes.

## 1.2 Schematic model for online quality control of the L-PBF process

Figure 1.1 illustrates a simplified flow chart of the system proposed for monitoring the process based on the AI decision-making of the deep learning classifier. As observed, the process parameters are placed as the input, and the system begins with depositing and executing a layer. As the layer is being executed, the system monitors the process and determines if there is a defect. If no defect exists, the system continues with the next layer or finishes the process. If there is a defect, the system determines if it is within a correctable threshold. If it's is correctable, it attempts to correct and repair it, but if not, it aborts the process and triggers an alarm.

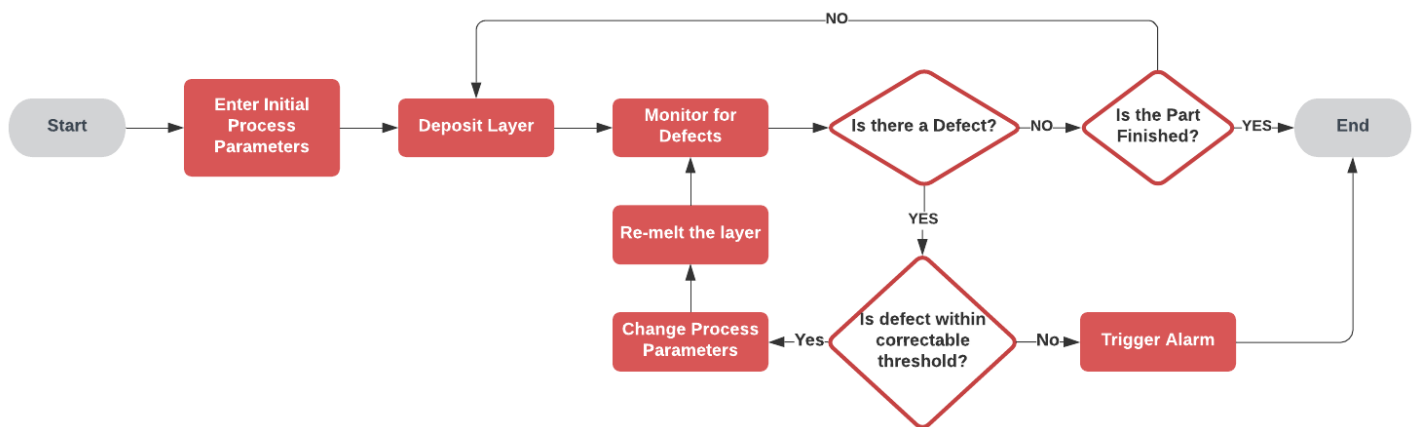


Figure 1.1 Flow chart for the online quality control of the L-PBF process.

### 1.3 Schematic AE setup for monitoring the L-PBF process

In order to monitor the L-PBF process, the AE sensor has been embedded beneath the build plate to minimize the distance between source and sensor. This setup could also provide a similar distance for each sample printing part to the sensor. Figure 1.2 shows the schematic of the AE setup in an L-PBF machine. Also, the ultimate monitoring system could have other outputs such as a Pyrometer and CCD camera.

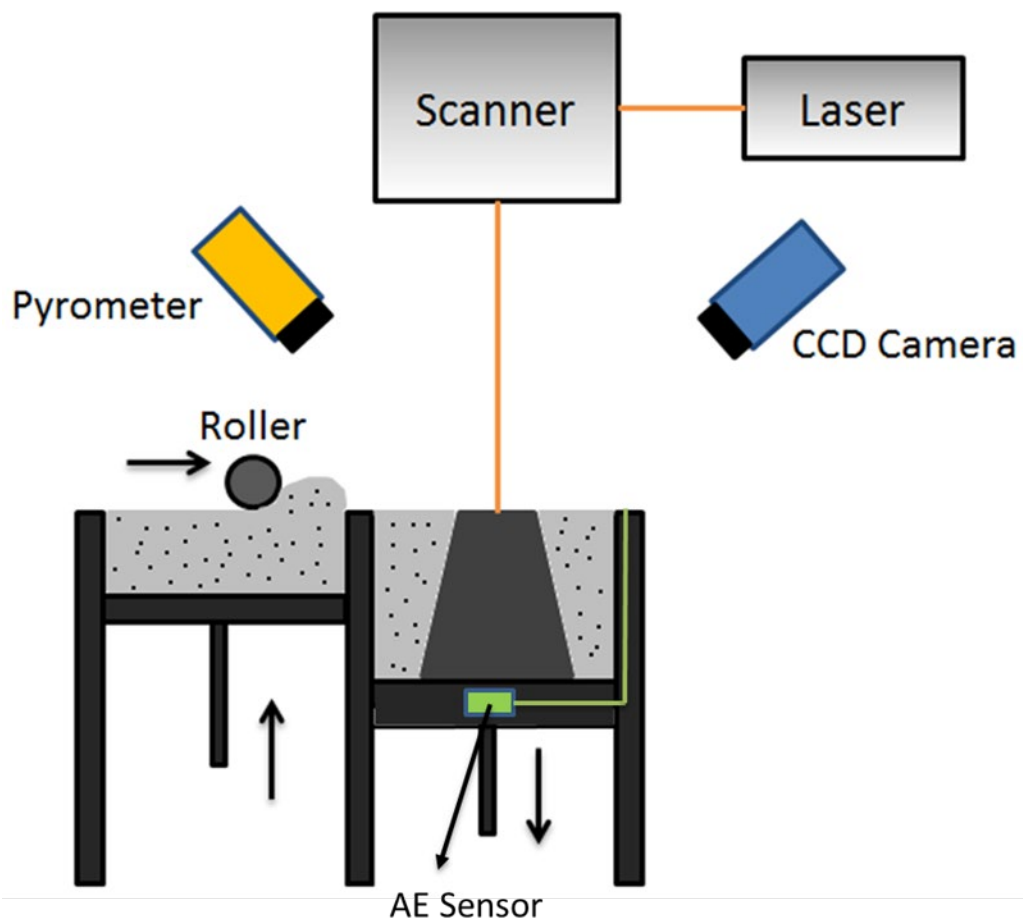


Figure 1.2 schematic of AE setup for monitoring L-PBF process

## 1.4 Research objectives

The main goal of this research project is to use Acoustic emission as an output for monitoring Laser powder Bed Fusion(L-PBF) via different machine learning methods to improve defect detection during Online monitoring.

The core objective of this work could be refined as the following:

- 1) Develop an acoustic emission sensor setup for monitoring the L-PBF process.
- 2) Process and analyze AE signals in different domains like the time and frequency domain.
- 3) Recognize patterns and classify AE signals with the goal of detecting defects in the monitoring L-PBF process.
- 4) Use Machine learning methods to produce a more general ML model for defect detection, one without material dependency.

## 1.5 Thesis outline

The main results of this thesis are a combination of two journal papers, which have already been published. The thesis is comprised of the following chapters:

**Chapter 1** introduces the background, motivation, and objectives of the research to frame the scope of the thesis.

**Chapter 2** is the first published journal article. This chapter targets the acoustic emission signals feature extraction in the time-domain and frequency-domain. Acoustic emission signals could be a good candidate for output in a monitoring system on L-PBF, as shown by the study on frequency domains via different machine learning methods (supervised and un-supervised methods). Moreover, the time domain signal's features show the repeatability of the acoustic emission signals in the steady-state of the printing process.

**Chapter 3** is the second published journal article. This chapter targets the application of machine learning on the acoustic emission signals in L-PBF. The potential of machine learning methods for monitoring the L-PBF process was shown using different machine learning methods based on the nature of each printed material. Moreover, the variational autoencoders suggested a new feature extraction method for having a more generalized data set. That leads to eliminating the material dependency in the training machine learning models.

**Chapter 4** summarizes the main conclusions and contribution of the thesis, highlights the strength and limitations, and presents suggestions for future work. Finally, this chapter outlines the contribution of this thesis to the literature.

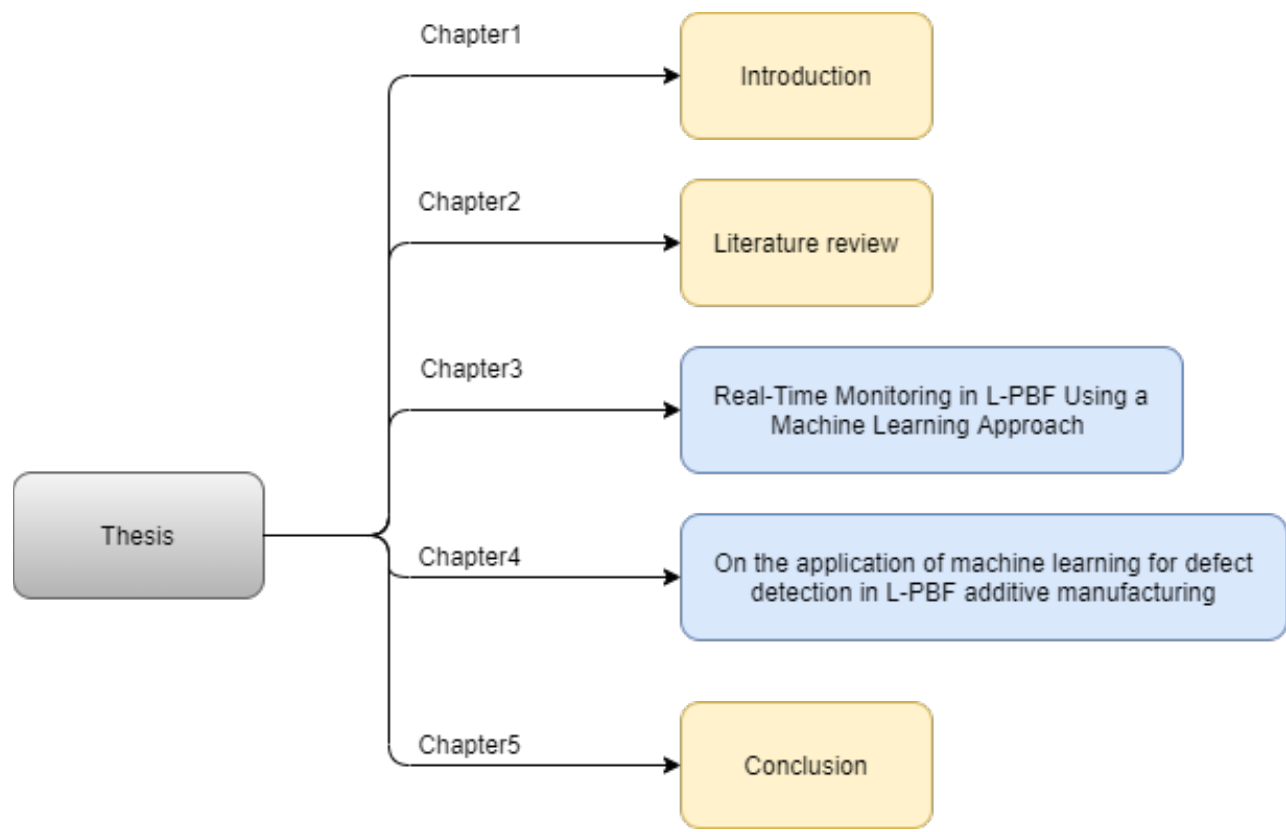


Figure 1.3 Structure of the thesis

## 1.6 References

1. Malekipour, E. and H. El-Mounayri, *Common defects and contributing parameters in powder bed fusion AM process and their classification for online monitoring and control: a review*. The International Journal of Advanced Manufacturing Technology, 2018. **95**(1-4): p. 527-550.
2. Abdelrahman, M., et al., *Flaw detection in powder bed fusion using optical imaging*. Additive Manufacturing, 2017. **15**: p. 1-11.
3. Purtonen, T., A. Kalliosaari, and A. Salminen, *Monitoring and adaptive control of laser processes*. Physics Procedia, 2014. **56**: p. 1218-1231.

## **Chapter 2**

### **Literature review**

## 2.1 Background

Nowadays, the machine learning method has received much attention due to its practicalities and benefits in various branches of science. One of the unique applications of this method can be found within monitoring laser powder bed fusion (L-PBF) additive manufacturing. Many components in industries are complicated in terms of geometry, and consequently, cannot be created using traditional manufacturing methods. The additive manufacturing (AM) approach has come to these complex geometries' aid and facilitated manufacturing. The L-PBF technique is considered a subfield of AM in which the raw material is powder, and a laser is used to fabricate the desired part.

In 2018, Yuan et al. employed a two-step machine learning method in this field and outlined the benefit of the obtained results for rapid evaluations of laser track welds[1]. L-PBF is also regarded as an additive manufacturing technique in which the metal parts are created layer by layer, and the powdered metals and alloys are melted through a high-power laser [2]. In another study, additive manufacturing was defined as a method to assemble and join materials with the aim of making parts from 3D model data[3]. Ivanna Baturynska et al. (2018) aimed to integrate the machine learning approach and finite element method (FEM) to optimize powder bed fusion additive manufacturing [4]. This combination can be helpful to simulate the process, optimize or anticipate the process parameters to obtain the specific mechanical properties. In addition, the developed models in the FEM were tested through this approach.

The research regarding the AM technique dates back to about twenty years ago [5]. However, the studies in this field need to be continued, and there are still concerns regarding this method's

practicalities and advantages. Baturynska et al. have illustrated the challenges in line with exploiting the machine learning method that is given below [4]:

- Such a tremendous amount of data needs to be considered in this method to have a precise performance.
- The data are gathered with too many difficulties, and the material costs for the experiment are remarkably high.

In another study, the three-dimensional bin-packing problems and nonconvex parts were defined considering the genetic algorithm used to optimize the part's orientation [5]. The parts contained holes and cavities and were machined through the Stereolithography AM process. Among all practicalities that have been introduced for machine learning so far, the fused deposition modelling (FDM) AM process has received much attention up to now [6].

A variety of machine learning methods have been proposed to model and simulate the AM process. There exists a considerable body of literature on the L-PBF AM process considering the machine learning approach [7-9]. These techniques that are used to simulate the L-PBF AM process are as follows: Artificial neural network, such as backpropagation neural network, and radial basis function neural network, based on fuzzy clustering and Pseudo-Inverse method, ensemble-MGGP including ANN, Bayesian classifier and support vector machine algorithm, the genetic algorithm like multi-gene genetic programming (MGGP), non-dominated genetic algorithm (NSGA-II), and multi-objective particle swarm optimizer, and support vector regression (SVR).

It is noteworthy that several machine learning (ML) methods can be utilized for a variety of purposes. In a significant study done by Sing et al. (2021), the main concern associated with the L-PBF technique is that the parts made from L-PBF do not have appropriate quality. One of the

unique challenges in using L-PBF is that it works with too many complications when fabricating the parts and that there are many oscillations. As a result, inconsistent parts are produced, which are not practical for the industry [10]. In this situation, the machine learning method can be employed to tackle such problems. Hence, the datasets are computed at different steps of the L-PBF process. Sing et al. (2021) combined the ML and L-PBF processes to monitor the quality and obtain acceptable results. Gobert et al., in 2018, also proposed a study that looked at the advantages of supervised machine learning to realize defects within metallic powder bed fusion additive manufacturing[11]. Notably, the image processing technique has been considered to monitor the additive manufacturing process using a high-resolution digital single-lens reflex (DSLR) camera. One significant positive aspect of this study is that the proposed approach prevents spending large sums of money on undesired products. Through this method, it is possible to check the quality and correct the defects during the build process.

In contrast, other computed tomography (CT) methods cannot realize the defects beforehand. Zhang et al. (2019) conducted a comprehensive investigation into the fatigue phenomenon and fracture behaviour of laser powder bed fusion stainless steel 316L [12]. In this study, the neuro-fuzzy method has been employed to predict fatigue life. The processing and post-processing strategies employed in studies play a prominent role in the number of variations in the severe cyclic fatigue phenomenon existing in the laser powder bed fusion materials. In addition, employing an effective and practical method to evaluate the fatigue property is a fundamental need. Zhang et al. (2019) attempted to anticipate the high cycle fatigue life of laser powder bed fusion stainless steel 316L using a neuro-fuzzy-based machine learning approach. The dataset considered in this study includes fatigue life data for the specimens under a variety of processing conditions (like laser

powder, scan speed, and layer thickness), cyclic stresses, and post-processing operations such as annealing and hot isostatic pressing. It is worth mentioning that the major usage of this data is related to simulating a complicated nonlinear input-output environment. The modes of crack creation and deformation were determined in this research.

One of the significant drawbacks of conventional methods is that they often fail to accurately create multi-scale, multi-material, and multi-functional products. Hence, the additive manufacturing method has emerged as a practical method to fabricate products and tackle the previous limitation. Despite such benefits, sometimes, the obtained products through AM differ considerably from the theoretical design expectations. A recent review of the literature on this topic (in 2020) [13] found that proposing some advanced algorithms and novel artificial intelligence methods can be significantly helpful to overcome the mentioned problems. In this review, Jin et al. aimed to illustrate enough information regarding the future of algorithm-driven additive manufacturing. Furthermore, several algorithms associated with the machine learning approach were examined and reviewed in detail. These algorithms were proposed to systematically overcome the three significant steps of the additive manufacturing process, namely geometrical design and process parameter configuration as well as in situ anomaly detection.

In order to summarize the AM's capabilities, four features are specified for this technique. They are as follows: (1) this method is known as the layer-by-layer process through which various shapes are fabricated; (2) hierarchical multi-scale structures ranging from the microstructure geometric to the part-scale macrostructure are designed and produced using this method; (3) a variety of material in the vast range of locations can be designed and produced; (4) an AM process is considered to fabricate fully functional assemblies and mechanisms directly.

Since there are many design variables with complex interactions over multiple domains, the AM's benefits have also delivered several challenges and defects. In a significant attempt in 2019, Xiong et al. aimed to study all these design variables and discussed their interactions [14]. In 2020, Jiang et al. introduced a ML integrated design for AM technique to illuminate the benefits of ML in learning the complicated relationships between the design and performance spaces. The AM technique considered in this study was employed to learn process-structure-property (PSP) relationships illustrated in. Finally, a case study was conducted to show the advantages of using ML in designing a customized ankle brace containing a tunable mechanical performance with tailored stiffness[15].

Recent years have seen many types of metal AM technologies that have been developed and employed in manufacturing fully functional parts. Some studies define seven groups for the technology that are as follows: binder jetting, direct energy deposition, material extrusion, material jetting, powder bed fusion (PBF), sheet lamination, and vat photopolymerization [16]. Hence, the basic theory and mechanism of AM technologies can vary considerably within the industry.

The steps that need to be considered in L-PBF are as follows: product design, process planning, L-PBF manufacturing, post-processing, and quality measurement. Some factors such as unsuitable quality assessment, inefficient process plan, and insufficient process control are the main reasons for inconsistency. On the other hand, to tackle such limitations, Liu et al. presented a new machine learning (ML)-enabled method employed to develop feedback loops in the whole metal L-PBF process. First, the metal L-PBF feedback loops were categorized, and a summary of the critical L-PBF manufacturing data was proposed for each step. Then, a generic framework of ML-enabled metal L-PBF feedback loops was introduced, and the feedback loops were individually defined in

detail. According to the obtained results, it was found that monitoring the closed-loop manufacturing for metal L-PBF can be possible using the ML-enabled feedback loops presented in this study(in 2020)[17].

The additive manufacturing (AM) process is also considered as three-dimensional printing within other studies. It is prevalent compared to the traditional subtractive manufacturing method due to the aforementioned reasons [18]. One of the significant drawbacks of the AM process is that this technique's parameters cannot be easily tuned. It has a remarkable impact on the printed microstructure and the subsequent products' performance. Hence, the conventional numerical and analytical models have mainly failed to create a process-structure-property-performance (PSPP) relationship for AM. Accordingly, presenting an effective approach for recognizing complicated patterns and analyzing regression irrespective of an explicit method is a fundamental need in order to construct and solve the most important physical models.

Interestingly, using the neural network (NN) to optimize the training process brings many benefits and is helpful in expediting the process. The NN has a large dataset, robust computational power, and complicated algorithm architecture. Qi et al. have considered this concept and finally reached acceptable results by suggesting the application of the NN algorithm to a number of steps in the AM process, such as model design, in situ monitoring, and quality assessment. The conclusions drawn in this study are also beneficial to those aiming to employ NNs in a vast range of applications like a conventional MLP for linking the AM technique, a conventional NN for AM melt pool recognition, and LSTM for creating FEM.

Moreover, direct metal deposition (DMD) is regarded as an AM technique in which many materials like steel or Titanium are employed to create the finished product [19]. The

computational methods and simulations have come to AM technique's aid and eliminated the trial and error involved in costly manufacturing processes. Through the use of finite element-based multi-physics simulation models (FEM), the AM process is assessed beforehand, and more limited parts can be used [20, 21]. Nevertheless, for computation purposes, the FEM-based simulations are not efficacious in terms of time and cost. In order to overcome this limitation, a predictive approach based on machine learning (ML) can be used to obtain simulation results and prevent conducting costly physics-based simulations. The physic-informed, data-driven, machine-learning systems can be employed to anticipate the AM processes' behaviour. Using this strategy increases the computation's speed in the multi-scale simulation tools, and real-time control systems are enhanced using in-situ data.

In 2019, Paul et al. designed and developed several important components in a scientific framework and extended a data-driven, model-based, real-time control system[22]. Through the use of FEM, the time-dependent thermal equations were solved, and the database was developed. One of the remarkable results of this study is that the proposed models can present mean absolute percentage errors of less than 1% for anticipating the temperature profiles for AM processes. One of the main aspects of quality evaluation in additive manufacturing (AM) is surface monitoring. Broadly speaking, engineers tend to realize the surface defects at the proper time during the AM process. In this case, the part is not subjected to undesired conditions and will not lose its quality. Concerning this concept, Chen et al. proposed a novel method to identify the surface defect rapidly for directed energy deposition (DED) in 2021 [23]. The major aim of this study was to develop an in-situ point cloud process using a machine learning approach that offered automatic surface monitoring without any sensor intermittence.

Moreover, machine learning and data informatics frameworks that were in line with detecting process-structure-property (PSP) relationships in the additive manufacturing process were discussed [24]. In this research, Kappes et al. attempted to create an ML framework with the aim of detecting the process structure and structure-property relationships during the AM process. The L-PBF was considered for manufacturing the Inconel 718, whose parameters were assessed in 3600 experiments. Based on the experimented samples, the pore formation was connected to part orientation, part location, and the usage of recycled powder. The random forest network machine learning model considered in the study was able to model the process-property and process-structure relationship in two ways and was expanded upon using data obtained from 3600 samples for the Inconel 718. The main steps considered for examining the L-PBF porosity and keyhole as well as fusion (LOF) defects in the specimen were examined in detail. Also, the striking effect of data collection, processing, and validation on the connections between input characteristics and output parameters associated with ML was examined.

It is noteworthy to mention the great importance and practicalities of metal additive manufacturing (AM) in the healthcare, aerospace, and automotive industry. According to the aforementioned explanations, there is no guarantee that reproducibility through AM can be obtained. This problem prevented others from developing a larger diffusion in industry. The machine learning method was proposed to deal with this problem as the manufacturing process is monitored simultaneously. As this technique is a layer-by-layer process, in-situ monitoring and the process of defects' identification can be very advantageous to prevent a waste of time and money. In 2021, D. Cannizzaro et al. aimed to present a system to monitor in-situ defects for metal powder bed fusion using an off-axis camera [25]. The algorithms considered in this research were based on computer

vision and machine learning that identified several powder bed defects and monitored the object's profile during the process.

There are various types of machine learning methods that can be employed in AM technology. For instance, Meng et al. employed a Gaussian process-based machine learning approach for L-PBF pf stainless steel [26]. In this research, the laser power was combined with laser scan speed in the L-PBF, and the re-melted depth of single tracks was anticipated. The numerical and experimental data were considered for training the GP model. The materials used in this process were 316L, and 17-4 PH stainless steel, and they were extended via the trained model. The main criterion considered in the study was the ratio of  $\Delta H/h_s$ , in which  $\Delta H$  denoted the specific enthalpy and  $h_s$  represented the enthalpy at melting. According to the results obtained in this study, the  $\Delta H/h_s \geq 30$  criterion was considered for the powder layer thickness in 316L.  $\Delta H/h_s \geq 25$  was considered for 17-4 PH.

Many techniques have been reported in the literature concerning monitoring the manufacturing process and defect identification. Some of these techniques have been mentioned above. Additionally, a support vector machine can also be advantageous for specifying the number of defects. These defects negatively affect the laser powder bed fusion and the fabricated metallic components' lifetime scatter. As a result, predicting the fatigue life of the engineering parts under the manufacturing process is an essential need. In 2020, Bao et al. employed a machine learning approach to identify the effect of defect location, size, and morphology on the lifetime of a selective laser melted Ti-6Al-4V alloy [27]. The high cycle fatigue post-mortem examination and synchrotron X-ray tomography were integrated with the aim of obtaining the geometric characteristics of the critical defects. Notably, the training of this process was conducted using

SVM. The results obtained in this study highlighted the fact that the maximum determination factor's value between the anticipated and experimental fatigue lives was 0.99. The SVM model has a remarkable capability for training in this field.

Previous studies have emphasized the applicabilities of acoustic-based monitoring in monitoring welding defects, identification of phase transformation, cracks formation, surface defects, and plasma formation [28]. Through the use of ML algorithms, it is possible to identify and categorize the defects of the welded melt pool rapidly[29]. In addition, existing studies represented the AE sensors' applications in monitoring the L-PBF process.

Kouprianoff et al. employed an ICP microphone attached to the wall of the build chamber to identify the defects and balling effects in single tracks of maraging steel and also compared two efficient and defective tracks in terms of powder layer thickness. Irrespective of using the ML algorithm, the difference in the energy over frequency between these tracks was accurately specified[30].

Using the L-PBF technique, Pandiyan et al. examined the various melting conditions of 316L laser tracks. A PAC AM41 sensor was mounted on the sidewalls of the build chamber to identify the airborne signals. Besides, a variety of processing for the raw AE signals was examined in this study. The authors stated that the frequency and time-frequency domains could also be considered to specify the different characteristics of the laser regimes[31].

Reider et al. employed the ultrasound sensor to monitor the L-PBF process and gather the related data layer by layer. A cylinder with an internal defect was examined in the study. On the lower side, a transducer was mounted, and it made it difficult to detect the longitudinal defects. The authors exploited the fast Fourier transform of the ultrasonic signals to examine the impact of

process parameters on the various layers. The results obtained in the study represented the ultrasound signals' capability for defect identification[32].

Ye et al. used a variety of ML algorithms in terms of time and frequency domain to collect the AE signal in a L-PBF process. Changing the laser scan speed and power, the balling, slightly balling, normal, and slightly overheating conditions were experimented for melting. In this research, a comparison was made between the multilayer perceptron (MLP) and support vector machine (SVM) technique based on the DBN classifier. The obtained results indicate the acceptable performance of SVM in classification for data after a FFT. Nevertheless, DBN has by far the best performance in the classification of raw data and is appropriate for fast decision-making and online control[33].

Wasmer et al. utilized a fibre Bragg grating AE sensor at the internal wall of the chamber to identify the airborne signals. Changing the laser scan speed, the various qualities were examined. In order to determine the frequency bands of the raw AE signals, a standard wavelet packet transform (WPT) was employed. Using this method, it is able to classify the various quality levels with up to 79-84% accuracy [34]. In a similar study, this classification rate reached 83-89% by using a fixed running window for the AE signal analysis [35]. The long and short running window method was experimented with twice with SCNN and presented higher classification accuracy. The same AE signals were classified employing an RL method to decrease the time required for training and data labelling. Although, the accuracy of classification was restricted to 74-82% [36].

Finally, in an advanced project, Eschner et al. exploited a piezoceramic sensor fixed under the build plate to monitor the L-PBF process. In order to define 54 cubes with various quality levels for the experiment, the laser power, scan speed, and hatch speed were changed. Short Fourier

transform was used on the raw AE data, and a spectrogram was gained for the layers and specimens. Three different classes were specified according to the number of specimens, and the background noise was eliminated from the spectrograms. Notably, a multilayer perceptron (MLP) was considered to classify the AE signals. The sigmoid function was used as an activation function for individual neurons and softmax for the output layer. The results obtained in this study represented the applicability of the proposed approach for classification with 76-86% accuracy. In contrast, the prediction accuracy for complex shapes was significantly lower [37, 38].

## 2.2 Potentials and challenges

AM can improve communication, training, and education in medical anatomical models. Anatomical models can include image anatomy acquisition, image processing, reconstruction using CT, and anatomical models prints [39, 40]. For having an accurate model image resolutions should be high as well. Also, It is possible to use material jetting techniques (such as polyjet) to material tune multi-material prints. ML algorithm can be trained with mechanical properties data and physician's input on haptic perception so that the model could help to achieve multi-material printing [41].

A new field in tissue engineering is Tissue engineering Bioprinting. This field focuses on prints bio-inks that fabricate tissue-like structures using 3D printing processes ((Khan et al. 2019 [42]; Mishbak et al. 2019 [43]). ML could predict the properties of the material by learning from large databases of designs and materials. Material properties can include the various mixture compositions of bio-inks to produce new scaffold designs for specific purposes (Yu and Jiang 2020

[44]. ML algorithms can lead to the Multiple objectives optimization of bio-ink prints, such as freeform reversible embedding.(Menon et al. (2019) [45]).

Numerous aspects like material, design and other processes can be covered by using ML in the 3D printing process of buildings and construction works (Lim et al. 2018[46]; Lao et al. 2020 [47]).

AM could play an essential role in having specific mechanical properties in building structures or particular interior design shapes. In addition, ML could help choose the process parameters based on the large dataset that came from the PSP of the material. Thus, ML can optimize material consumption, learn process plans, and reduce build time by contrasting the cost of the numerous plans [41].

Since the late 1980s, the automotive industry has used AM to design and redesign car components. A wide range of prototypes have been printed at the product development stage and are used for negotiations and evaluations. AM is also an attractive solution as customization becomes increasingly important. This is because of its ability to tailor-make products, which conventional techniques have difficulty doing. AM was used to print car interior prototypes intended for testing and communication purposes. This is in contrast to conventional techniques, such as plastic injection moulding, that were used to manufacture actual car components[48].

The interior design of a car often influences sales. With customizable interiors available, buyers can personalize according to their taste and budget, which boosts car sales. Printed parts can now be more frequently used in actual cars since AM is capable of meeting the demands of the variations within customization. Dashboards with the same dimensions are printed in smaller sections before being glued together and coated with acrylic paint. SLA has high printing accuracy,

which allows the seamless fitting of separate sections and the fabrication of functionally fitted parts. The working airbox of an engine can also be printed via SLA. Due to the high temperature produced during combustion, thermoset polymers capable of withstanding this tremendous heat are selected for the printing process[48].

AM is currently used in all stages of the aircraft manufacturing industry, from the initial design to the final production of the aerospace components. AM is also used for repairs and support systems. The ever-increasing use of AM techniques is observed in aerospace original equipment manufacturers (OEMs), as well as maintenance, repair, and overhaul (MRO) companies. Complete assemblies or special design requirements for a component are often desired in the aerospace industry. These needs can easily be met with AM's agility and empowerment within small and medium-sized enterprises. This would allow these enterprises to compete with big companies[48].

To produce hollow composite components, composite materials can be wrapped around 3D printed soluble cores. One example of this process is the fabrication of unmanned vehicle capsules. AM would eliminate the need for tooling works in repair and small-scale manufacturing, thereby reducing what makes up the majority of the overall cost. Compared to the weeks needed for conventional manufacturing methods, manufacturing tools like moulds, jigs, surrogates, fixtures, and templates can be printed in a matter of hours. For example, the building of polycarbonate wiring conduits through FDM can take less than three days and be done at a small price. In contrast, a similar aluminum cast component would take more than six weeks to produce[48].

Airlines can also have different needs for their aircraft interiors. Boeing, an aircraft manufacturing company, would print customizable interiors for its aircraft. It will be time-consuming to make these customizations conventionally. It is not justifiable to produce a few copies at such a high price. General Electric Aviation saves on fuel consumption by reducing engine weight using 3D printing technology[48].

Manufacturers equipped with 3D printers have the ability to gain demanding business opportunities not achievable with conventional manufacturing techniques. AM's flexibility allows manufacturers to adjust product designs at any time point by editing the CAD file. AM focusing on small to medium-sized prototyping business opportunities brought about the revolution of conventional injection moulding techniques. The tooling cost of injection mouldings is high, and the development and building process is time-consuming. With AM, it is possible to import a CAD file to a machine and print a part within hours. Even if the part is large or has complex geometries, it will take a maximum of several days to complete. Traditional manufacturing would take weeks or even months. Competition within the traditional manufacturing sector is tough, but companies can use 3D printing to secure business via the development, design, proof, or prototyping phases of the idea as opposed to quick production turnarounds. This enables companies to communicate more effectively with clients throughout the prototype development and production stages[48].

In ML techniques, data-driven numerical simulations are more efficient (computationally) versus the more physics-based numerical simulations. A trained ML model gives stress predictions for lattice structures in 0.47 s while FEM simulations take five to ten hours (in 2018) [49]. However, training large data sets is time-consuming and computationally expensive.

The computational cost could be an important factor within in situ monitoring and closed-loop control. Real-time layer-by-layer defect detections and melt pool inspections need to detect defects spontaneously in order to not increase build time or significantly affect production rates. Since printing a layer takes several minutes to finish, the detection operation is considered to be fast acting. However, melt pool inspections with high-speed cameras need more computational power because of the larger data set. Better ML techniques are required for these kinds of applications to compensate for the large data set. thermal-mechanical models were studied using high-performance computations known as Convolutional (Francis and Bian, 2019) [50]. Artificial Neural Networks for Additive Manufacturing Predictions were used via Big Dat deep learning algorithms (CAMP-BD). A large sum of thermal images were captured, equivalent to 40 GB of data. The supercomputer cluster at Mississippi State took 26 days to train the Deep learning model[41].

### **2.3 Standardization requirements in ML**

Sharing data is necessary in order to develop an extensive database, something that is needed to run ML algorithms. In addition, many researchers are working on novel materials and process development stages. The standards are seen within data acquisition, and the pre-processing of data would encourage data sharing and improve collaboration amongst the AM community. Unfortunately, the ML frameworks in the market like TensorFlow, Cafe, and Pytorch are not compatible. As a result, a uniform framework is required to allow the sharing of machine learning models. [41].

## 2.4 Summary

It is evident through the literature review that process monitoring and inspection systems are needed to improve the AM process' quality. Existing monitoring and inspection systems for AM processes typically focus on measuring process signatures like melt pool temperature and geometry. Thermal and vision-based imaging techniques have served excellently for predicting AM part quality. The collection of process signature data can be performed effectively and accurately with the advancements seen in measurement science and technology, the specification of IR and CCD cameras. Based on the accurate process signature data, further studies could lead to a more precise correlation between process parameters and signatures. For example, there is little focus on data processing and measurement error evaluation. This can lead to uncertainty in the melt pool geometry and temperature measurements. Minimizing measurement errors will help reach the necessary accuracy levels in developing a process control system. Using a numerical simulation method, a predictive model for metal-based AM processes should be developed to get the melt pool's geometric information [51]. Currently, the numerical method can simulate a single track and simple geometries, which demonstrates the limited representation of melt pool dynamics. Further studies for a simulation technique should be performed to get the geometric information of the melt pool in multi-layers or multi-track. Based on the studies stated above, process monitoring, inspection systems, and control algorithms should be developed. Control algorithms specifically could be used to develop the real-time closed-loop system[52]. Same as the melt pool measurement, other measurements, such as acoustic signals, acoustic emission signals, temperate and etc. need to have more focus on data processing and in the case that there isn't any mathematical model for the simulation, the AI can be a good candidate to create a model for

detections and prediction. Due to the sensitivity of AE technique and cost-effective method in comparison of IR camera or high speed- high resolution camera, it could be an effective method for quality control in the AM industry. It should be mentioned, although it is simple in principle, it can be difficult to implement. First, the characteristic of the emitted signal is unpredictable, as is greatly dependent on the source material. Second, the mechanism by which acoustic emission works unfortunately applies to noise as well. Depending on the positioning and setup, it is possible for different signals to be detected.

## 2.5 References

1. Yuan, B., et al., *Machine-Learning-Based Monitoring of Laser Powder Bed Fusion*. Advanced Materials Technologies, 2018. **3**(12): p. 1800136.
2. Yap, C.Y., et al., *Review of selective laser melting: Materials and applications*. Applied physics reviews, 2015. **2**(4): p. 041101.
3. ISO, A., *Standard Terminology for Additive Manufacturing—General Principles—Terminology*. 2015.
4. Baturynska, I., O. Semeniuta, and K. Martinsen, *Optimization of process parameters for powder bed fusion additive manufacturing by combination of machine learning and finite element method: A conceptual framework*. Procedia Cirp, 2018. **67**: p. 227-232.
5. Ikonen, I., et al. *A Genetic Algorithm for Packing Three-Dimensional Non-Convex Objects Having Cavities and Holes*. in *ICGA*. 1997.
6. Garg, A., K. Tai, and M. Savalani, *State-of-the-art in empirical modelling of rapid prototyping processes*. Rapid Prototyping Journal, 2014.
7. Garg, A., J.S.L. Lam, and M. Savalani, *A new computational intelligence approach in formulation of functional relationship of open porosity of the additive manufacturing process*. The International Journal of Advanced Manufacturing Technology, 2015. **80**(1): p. 555-565.
8. Wang, R.-J., et al., *ANN model for the prediction of density in selective laser sintering*. International Journal of Manufacturing Research, 2009. **4**(3): p. 362-373.
9. Wang, R.-J., et al., *Influence of process parameters on part shrinkage in SLS*. The International Journal of Advanced Manufacturing Technology, 2007. **33**(5): p. 498-504.
10. Sing, S., et al., *Perspectives of using machine learning in laser powder bed fusion for metal additive manufacturing*. Virtual and Physical Prototyping, 2021. **16**(3): p. 372-386.
11. Gobert, C., et al., *Application of supervised machine learning for defect detection during metallic powder bed fusion additive manufacturing using high resolution imaging*. Additive Manufacturing, 2018. **21**: p. 517-528.
12. Zhang, M., et al., *High cycle fatigue life prediction of laser additive manufactured stainless steel: A machine learning approach*. International Journal of Fatigue, 2019. **128**: p. 105194.
13. Jin, Z., et al., *Machine learning for advanced additive manufacturing*. Matter, 2020. **3**(5): p. 1541-1556.
14. Xiong, Y., et al., *Data-driven design space exploration and exploitation for design for additive manufacturing*. Journal of Mechanical Design, 2019. **141**(10).
15. Rosen, D.W., *Research supporting principles for design for additive manufacturing: This paper provides a comprehensive review on current design principles and strategies for AM*. Virtual and physical prototyping, 2014. **9**(4): p. 225-232.
16. Astm, I., *ASTM F2900-15 standard terminology for additive manufacturing—general principles—terminology*. ASTM International, West Conshohocken, PA, 2015. **3**(4): p. 5.
17. Liu, C., et al., *Machine Learning-enabled feedback loops for metal powder bed fusion additive manufacturing*. Procedia Computer Science, 2020. **176**: p. 2586-2595.
18. Qi, X., et al., *Applying neural-network-based machine learning to additive manufacturing: current applications, challenges, and future perspectives*. Engineering, 2019. **5**(4): p. 721-729.
19. Ding, Y., J. Warton, and R. Kovacevic, *Development of sensing and control system for robotized laser-based direct metal addition system*. Additive Manufacturing, 2016. **10**: p. 24-35.
20. Yan, W., et al., *Data-driven multi-scale multi-physics models to derive process–structure–property relationships for additive manufacturing*. Computational Mechanics, 2018. **61**(5): p. 521-541.
21. Ding, J., et al., *Thermo-mechanical analysis of Wire and Arc Additive Layer Manufacturing process on large multi-layer parts*. Computational Materials Science, 2011. **50**(12): p. 3315-3322.

22. Paul, A., et al. *A real-time iterative machine learning approach for temperature profile prediction in additive manufacturing processes*. in *2019 IEEE International Conference on Data Science and Advanced Analytics (DSAA)*. 2019. IEEE.
23. Chen, L., et al., *Rapid surface defect identification for additive manufacturing with in-situ point cloud processing and machine learning*. *Virtual and Physical Prototyping*, 2021. **16**(1): p. 50-67.
24. Kappes, B., et al. *Machine learning to optimize additive manufacturing parameters for laser powder bed fusion of Inconel 718*. in *Proceedings of the 9th International Symposium on Superalloy 718 & Derivatives: Energy, Aerospace, and Industrial Applications*. 2018. Springer.
25. Cannizzaro, D., et al. *Image analytics and machine learning for in-situ defects detection in Additive Manufacturing*. in *2021 Design, Automation & Test in Europe Conference & Exhibition (DATE)*. 2021. IEEE.
26. Meng, L. and J. Zhang, *Process design of laser powder bed fusion of stainless steel using a gaussian process-based machine learning model*. *JOM*, 2020. **72**(1): p. 420-428.
27. Bao, H., et al., *A machine-learning fatigue life prediction approach of additively manufactured metals*. *Engineering Fracture Mechanics*, 2021. **242**: p. 107508.
28. Sun, A., E. Kannatey-Asibu Jr, and M. Gartner, *Sensor systems for real-time monitoring of laser weld quality*. *Journal of Laser Applications*, 1999. **11**(4): p. 153-168.
29. Saad, E., H. Wang, and R. Kovacevic, *Classification of molten pool modes in variable polarity plasma arc welding based on acoustic signature*. *Journal of materials processing technology*, 2006. **174**(1-3): p. 127-136.
30. Kouprianoff, D., et al. *Acoustic emission technique for online detection of fusion defects for single tracks during metal laser powder bed fusion*. in *Solid Freeform Fabrication Symposium, University of Texas at Austin*. 2018.
31. Pandiyan, V., et al., *Analysis of time, frequency and time-frequency domain features from acoustic emissions during Laser Powder-Bed fusion process*. *Procedia CIRP*, 2020. **94**: p. 392-397.
32. Rieder, H., et al. *On-and offline ultrasonic characterization of components built by SLM additive manufacturing*. in *AIP Conference Proceedings*. 2016. AIP Publishing LLC.
33. Dong, G., J. Marleau-Finley, and Y.F. Zhao, *Investigation of electrochemical post-processing procedure for Ti-6Al-4V lattice structure manufactured by direct metal laser sintering (DMLS)*. *The International Journal of Advanced Manufacturing Technology*, 2019. **104**(9): p. 3401-3417.
34. Wasmer, K., et al. *In situ and real-time monitoring of powder-bed AM by combining acoustic emission and artificial intelligence*. in *International Conference on Additive Manufacturing in Products and Applications*. 2017. Springer.
35. Shevchik, S.A., et al., *Acoustic emission for in situ quality monitoring in additive manufacturing using spectral convolutional neural networks*. *Additive Manufacturing*, 2018. **21**: p. 598-604.
36. Wasmer, K., et al., *In situ quality monitoring in AM using acoustic emission: A reinforcement learning approach*. *Journal of Materials Engineering and Performance*, 2019. **28**(2): p. 666-672.
37. Eschner, N., et al., *Classification of specimen density in Laser Powder Bed Fusion (L-PBF) using in-process structure-borne acoustic process emissions*. *Additive Manufacturing*, 2020. **34**: p. 101324.
38. Eschner, N., et al. *Development of an acoustic process monitoring system for selective laser melting (SLM)*. in *Proceedings of the 29th Annual International Solid Freeform Fabrication Symposium, Austin, TX, USA*. 2018.
39. Van Eijnatten, M., et al., *CT image segmentation methods for bone used in medical additive manufacturing*. *Medical engineering & physics*, 2018. **51**: p. 6-16.
40. Radzi, S., et al., *Development of a three-dimensional printed heart from computed tomography images of a plastinated specimen for learning anatomy*. *Anatomy & cell biology*, 2020. **53**(1): p. 48.

41. Goh, G.D., S.L. Sing, and W.Y. Yeong, *A review on machine learning in 3D printing: applications, potential, and challenges*. Artificial Intelligence Review, 2021. **54**(1): p. 63-94.
42. Khan, Z., et al., *Optimization of a 3D bioprinting process using ultrashort peptide bioinks*. International Journal of Bioprinting, 2019. **5**(1).
43. Mishbak, H., G. Cooper, and P. Bartolo, *Development and characterization of a photocurable alginate bioink for three-dimensional bioprinting*. International Journal of Bioprinting, 2019. **5**(2).
44. Yu, C. and J. Jiang, *A perspective on using machine learning in 3D bioprinting*. International Journal of Bioprinting, 2020. **6**(1).
45. Menon, A., et al., *Optimization of silicone 3D printing with hierarchical machine learning*. 3D Printing and Additive Manufacturing, 2019. **6**(4): p. 181-189.
46. Tan, K. *The framework of combining artificial intelligence and construction 3D printing in civil engineering*. in MATEC web of conferences. 2018. EDP Sciences.
47. Lao, W., et al., *Improving surface finish quality in extrusion-based 3D concrete printing using machine learning-based extrudate geometry control*. Virtual and Physical Prototyping, 2020. **15**(2): p. 178-193.
48. Chua, C.K., C.H. Wong, and W.Y. Yeong, *Standards, quality control, and measurement sciences in 3D printing and additive manufacturing*. 2017: Academic Press.
49. Koeppe, A., et al., *Efficient numerical modeling of 3D-printed lattice-cell structures using neural networks*. Manufacturing Letters, 2018. **15**: p. 147-150.
50. Francis, J. and L. Bian, *Deep learning for distortion prediction in laser-based additive manufacturing using big data*. Manufacturing Letters, 2019. **20**: p. 10-14.
51. Lei, N., et al., *An additive manufacturing process model for product family design*. Journal of Engineering Design, 2016. **27**(11): p. 751-767.
52. Chua, Z.Y., I.H. Ahn, and S.K. Moon, *Process monitoring and inspection systems in metal additive manufacturing: Status and applications*. International Journal of Precision Engineering and Manufacturing-Green Technology, 2017. **4**(2): p. 235-245.

## **Chapter 3**

### **Real Time Monitoring in L-PBF Using a Machine Learning Approach**

#### **Complete Citation:**

Mohammadi, Mohammad Ghayoomi, and Mohamed Elbestawi. "Real Time Monitoring in L-PBF Using a Machine Learning Approach." Procedia Manufacturing 51 (2020): 725-731.

**Abstract:**

Laser powder bed fusion (L-PBF) is an additive manufacturing process whereby a heat source (laser) is used to consolidate material in powder form to build three-dimensional parts. This paper uses real-time monitoring in L-PBF for quality control. Acoustic Emission (AE) is used to detect various defects like pores and cracks during the powder bed selective laser melting process via the machine learning approach. Data collection is performed under various process parameters, using an AE sensor. Several time and frequency-domain features are extracted from the AE signals during data mining. K-means clustering is employed during the unsupervised learning, and a neural network approach is employed for the supervised machine learning on the dataset. Data labelling is conducted for different laser powers, clustering results and signal time durations. The results show the potential of real-time quality monitoring using AE during the L-PBF process.

**Keywords:**

Powder bed fusion; K-means; Acoustic Emission

### 3.1 Introduction

Additive Manufacturing (AM) is a promising technology used to fabricate complex geometries which are difficult or impossible to manufacture through conventional manufacturing routes. A sub-field of AM, known as Laser Powder Bed Fusion (L-PBF), uses powder as the raw material, along with a heat source (laser) to fabricate the desired part. Owing to its unique capabilities, L-PBF has attracted the attention of different industrial sectors [1]. The increasing demand for performance improvement in various industries has motivated design innovation [2]. AM technologies are particularly suited to deal with these increasing market requirements. Despite its huge demand, lack of repeatability is one of the biggest issues in the application of L-PBF within various industries. Therefore, improving the quality and repeatability within AM technology is an important objective.

Even if the same process parameters are used, it is challenging to produce parts with the same mechanical properties. Despite significant advancements in AM technology, microstructure defects such as porosity, material supply issue, cracks, vaporization and etc. persist and are the main contributors to the existing lack of repeatability. The presence of such an issue is attributed, at least in part, to insufficient in-process monitoring and closed-looped control algorithms of machine operations. Additional modules can be added to AM machines to store generated data in real-time for the closed-loop feedback. Some closed-loop feedback equipment includes high-speed CMOS-camera (PBF process for melt pool monitoring), dual-colour pyrometer (Directed Energy Deposition(DED) for melt pool monitoring and build height), and in-line coherent imaging (DED for depth measurement)[3].

The purpose of this paper is to address the problem of lack of repeatability during the L-PBF for on-line process monitoring by using Acoustic Emission (AE). AE creates transient electric waves by quickly releasing localized energy, thereby capturing information on subsurface dynamics occurring during the process. Examples include fracture, plastic deformation, and crack initiation and growth[4]. For example, for pipe rupture research, AE is applied to examine flaws in pressure vessels and stress corrosion cracking among others. AE is exceptionally sensitive, detecting crack growth of  $25\mu\text{m}$  compared to the  $0.55\text{ mm}$  growth detected by ultrasonic and radioactive testing[5]. AE monitoring also identifies growing flaws with magnitudes smaller than any other non-destructive test technique (NDT)[5].

Alongside its exceptional sensitivity, AE is more applicable than other techniques for monitoring and evaluating structural integrity. This is due to its potential for continuous monitoring, warning indications, complete component volume inspection, and the identification of crack initiation, propagation, and leaks. Using an array of AE sensors, the global area or the volume of components can be assessed without the use of time-consuming and high-cost scanning[4].

The characteristics of the AE signal depend on the defect itself, and therefore, can be correlated to its occurrence. However, the AE signal cannot predict any upcoming changes in the characteristics of the defects (e.g. size) in advance. In addition, the characteristics of the AE signal depend on the path between the defect and the source[4].

The AE data can be acquired via the AE system, which is comprised of a pre-amplifier, a data acquisition, and AE sensors. After collecting time-domain waves, AE features need to be extracted from the raw wave data. The AE features could be in the time-domain, frequency-domain, or time-frequency-domain. The main purpose behind collecting data and feature extractions is using them

for online investigations, where the using waves created by defects and those created via perfect solidification can be distinguished.

Previous monitoring methods have primarily focused on the experimental setup and variable measurements. Studies have rarely employed intelligent process monitoring for defect detection. In-situ monitoring processes require faster speeds, higher recognition accuracy, and fewer computational cost. Intelligent methods are widely applied in defect detection and manufacturing process monitoring [6, 7]. An artificial intelligent method would be a good candidate for classifying wave sources. Thus, monitoring the L-PBF process by AE signal via a machine learning method is proposed.

This study includes three parts. The first is looking at the Time-Domain data and analyzing AE signals for the entire printing process. Afterwards, all waveforms were transferred to the frequency-domain. They were then used as input for the K-Means clustering to produce more information from the dataset. Lastly, the deep learning method was used to categorize AE signals, which helps in the control system of the L-PBF machine.

At the end, the deep learning model is already prepared and requires the input of information. The deep learning model can classify AE signals in each layer, a procedure which includes transferring all waveforms to the frequency-domain and using them as test data. The result can help to change input for the next layers or for the last printed layer to melt again. After inputting new process parameters, the L-PBF will continue printing parts.

## 3.2 Experimental procedures

### 3.2.1 Feedstock materials

The starting material was gas-atomized stainless steel 316 L powder (Carpenter Technology LTD) with particle sizes in the 15–45 $\mu\text{m}$  range. The particle size distribution (PSD) of the received and sieved powder was measured through the laser diffraction method using a Malvern Master sizer 2000.

### 3.2.2 Selective laser melting processing

An OmniSint-160 SLM machine equipped with a 400 W laser was used to produce test samples. In all samples, the layer thickness, hatch spacing and scanning speed were set at 0.04 mm, 0.08 mm, and 600 mm/sec, respectively. Laser power and energy density for each sample are listed in Table 3-1. During each run, eight cylindrical parts with a 10 mm radius of and a 10 mm height were produced (Figure 3.1). Samples were directly fabricated on the build plate without any post-processing. The cylinders were then removed using wire-cut Electrical Discharge Machining (EDM).



Figure 3.1. Printed parts on the build plate.

Table 3-1 laser power and energy density of each test sample.

Sample number	Laser power (W)	Energy density (J/mm <sup>3</sup> )
1	75	39.06
2	100	52.08
3	150	78.13
4	180	93.75
5	200	104.16
6	220	114.58
7	250	130.2
8	300	156.25

### 3.2.3 AE system

The AE system used in this experiment is a WSα, 100-900 kHz wideband frequency sensor connected to a USB-ae node. The USB Node is a full-featured, low-cost Acoustic Emission System that plugs conveniently into the USB Port of the User's PC or laptop. All filtering parameters for the AE system acquisition are listed in Table 3-2. The sensor was attached to the center of and underneath the build plate. In order to maintain the same distance between parts and sensor, all parts were placed within a 4 cm radius circle. The pencil lead break method was used prior to each test according to the ASTM E976-1025 standard in order to calibrate the AE sensor. Vacuum grease was used to cover the contact surface between specimens and sensor to produce proper acoustical coupling. There was a time gap for melting each part in each layer to distinguish each part's wave easily.

Table 3-2AE system filtering parameters.

Threshold		Analog Filter		Waveform Setup	
Type	dB	Lower	Upper	Sample Rate	Pre-trigger
FIXED	40	20kHz	1MHz	5MSPS	16.00

### 3.2.4 K-Means Clustering algorithm[8]

One of the most conventional methods for exploratory data analysis is clustering. In this study the K-means algorithm was used since it is an efficient classifier for data points with predefined number of clusters. It is also fast enough for use on large amounts of data and aids in producing a meaningful intuition of the data structure. Furthermore, this method has been used in previous acoustic signal research [9]. The K-means objective function is one of the most popular clustering analyses within data mining. K-means clustering is a vector quantization method, originally drawn from signal processing. In K-means, data is segregated into disjoint sets  $C_1, \dots, C_k$  where a centroid denotes each  $\mu_i$ , partitioning  $n$  observations into K clusters such that each observation fits into the cluster with the closest mean. The purpose is to create a cluster prototype, and the result is that data space is partitioned. K-Means minimizes the variances within each cluster, which is represented as squared Euclidean distances. The assumption is that the input set is embedded within some large metric space  $(X', d)$  (so that  $X \subseteq X'$ ) and the centroids are members of  $X'$ . The objective function of K-means measures the squared distance between the centroid of the cluster and each point in  $X$ . The centroid of  $C_i$  is defined as:

$$\mu_i(C_i) = \arg \min_{\substack{X \in C_i \\ \mu \in X'}} \sum d(x, \mu)^2 \quad 3.1$$

The k-means objective is defined as:

$$G_{k\text{-means}}((X, d), (C_1, \dots, C_k)) = \sum_{i=1}^k \sum_{x \in C_i} d(x, \mu_i(C_i))^2 \quad 3.2$$

which can also be rewritten as the following:

$$G_{k\text{-means}}((X, d), (C_1, \dots, C_k)) = \min_{\mu_1, \dots, \mu_k \in X'} \sum_{i=1}^k \sum_{x \in C_i} d(x, \mu_i)^2 \quad 3.3$$

### 3.2.5 Deep learning for classification

Layers, input data, loss functions, and optimizers are all components of neural network training. The layers form the network, while the input data targets the network, comprised of chained layers to map the input data into predictions. The loss function compares the predictions to its targets and produces a loss value, which measures how well the predictions match expectations. The optimizer updates the network's weights by using the loss value [10]. An epoch is the number of times in which all training vectors are used, such that it updates the weights. In batch training, all training samples simultaneously go through the learning algorithm within one epoch before updating weights. In sequential training, all weights are updated after the sequential passing of each vector through the training algorithm (Figure 3.2).

The used model had five layers; all of them were fully connected (Table 3-3). To train the model, categorical cross-entropy was the loss function and Adam was the optimizer. Categorical cross-entropy for K class and n samples can be calculated as:

$$L(y_{true}, y_{predict}) = \sum_i^n \sum_k^K -y_{true}^{(k)} \log(y_{predict}^{(k)}) \quad 3.4$$

The accuracy of the model is computed by simply counting the number of correct predictions divided by the total number of samples, which gives a number in [0,1]. Figure 3.3 shows the training's loss value and accuracy. The test part contained 15% of the data set.

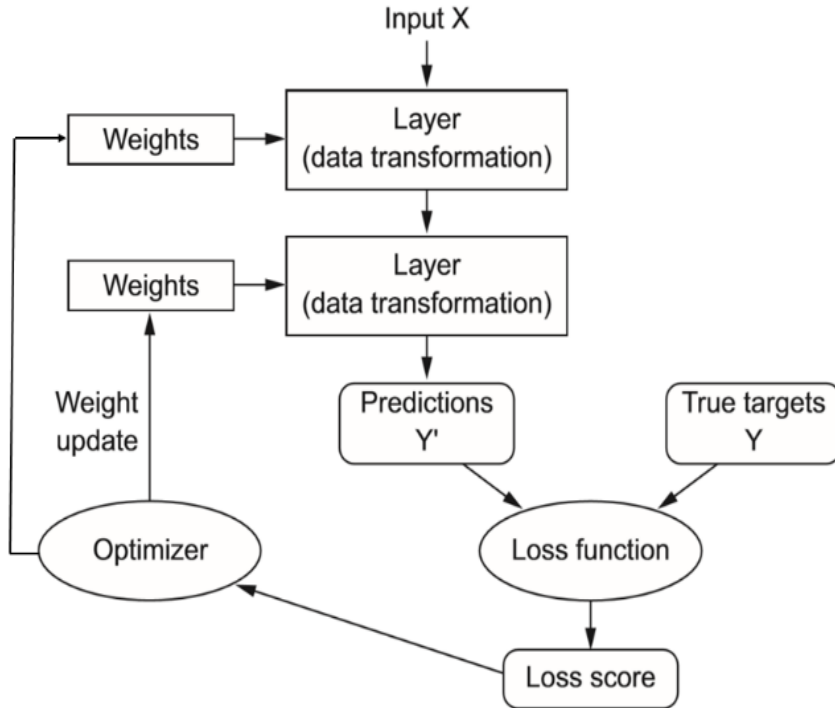
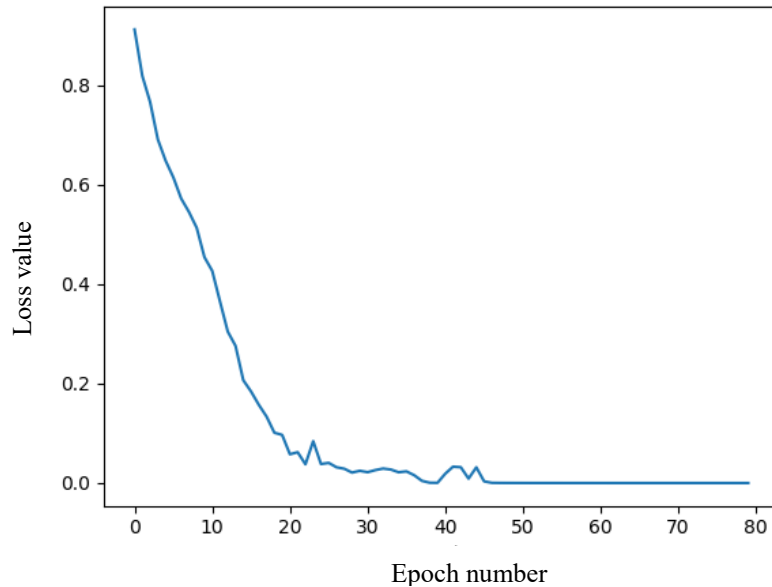


Figure 3.2 Schematic of layers, networks, loss function, and optimizer in a deep learning model [10]

Table 3-3 Details of layers, networks in the deep learning model.

Layer (type)	Output Shape	Number of Parameters
dense_1 (Dense)	(None, 2000)	7172000
dense_2 (Dense)	(None, 1000)	2001000
dense_3 (Dense)	(None, 400)	400400
dense_4 (Dense)	(None, 220)	88220
dense_5 (Dense)	(None, 3)	884

(a)



(b)

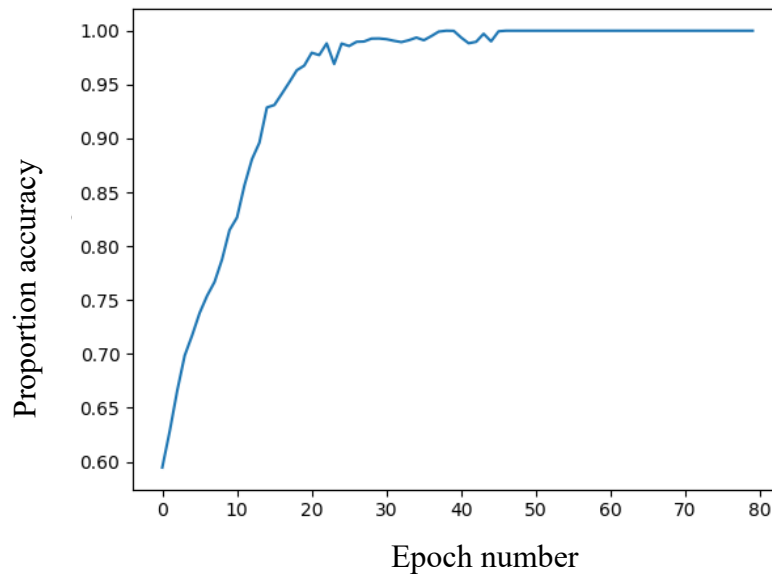


Figure 3.3(a) Loss value and (b) accuracy in each epoch in the training part

### 3.3 Results

#### 3.3.1 Time-domain data responses for the whole printing process

Time-domain AE signal features are listed in Table 3-4. As shown in Figure 3.5, there is a significant difference in time-domain data, such as the number of counts, energy, and rise time during the printing of the first layers and the rest of the layers. Based on the time, it was noted that the first 20 layers have a significant difference, and accordingly, the data from these layers are not reliable to be used in the machine learning methods. This transient behaviour can be explained as follows:

First, thermal transient behaviour in printing the first few layers can occur due to the difference in the cooling rate of these layers and subsequent ones can be caused by various cooling mechanisms [11]. To clarify, the initial layers are in direct contact with the cold substrate, which acts as a heat sink. However, the subsequent layers are consolidated on the heated layers which were previously deposited. Second, the powder layer thickness during the L-PBF processes deviates from the initial value due to the difference between the thickness of the deposited powder layer before and after consolidation. The liquid formed after the melting of the powder particles fills the inter-particle pores and creates a dense layer that is lower in thickness compared to the initial deposited layer [12]. The powder layer thickness approaches a constant value known as effective powder layer thickness and remains unchanged during the rest of the printing process. The third reason behind this transient behaviour, shown in Figure 3.6, is the fact that the travelling path of the waves towards the sensor is very different for the first layers compared to the rest of the layers. The enhanced dissipation of AE signals occurs due to the presence of powder particles surrounding the build which are believed to reduce the intensity of time-domain features.

Moreover, as shown in Figure 3.6, the waves travel a longer distance for the first layers to reach the sensor.

Table 3-4 Time-domain AE signal features with their definition.

Feature	Definition
peak amplitude	The highest measured voltage in a waveform
number of counts	Numbers that the signal crossed at the threshold
duration	The time difference between the crossing of the first and last threshold
energy	The area under the voltage-time graph, specifically within a set duration
rise time	The interval time between the first threshold crossing and the signal peak

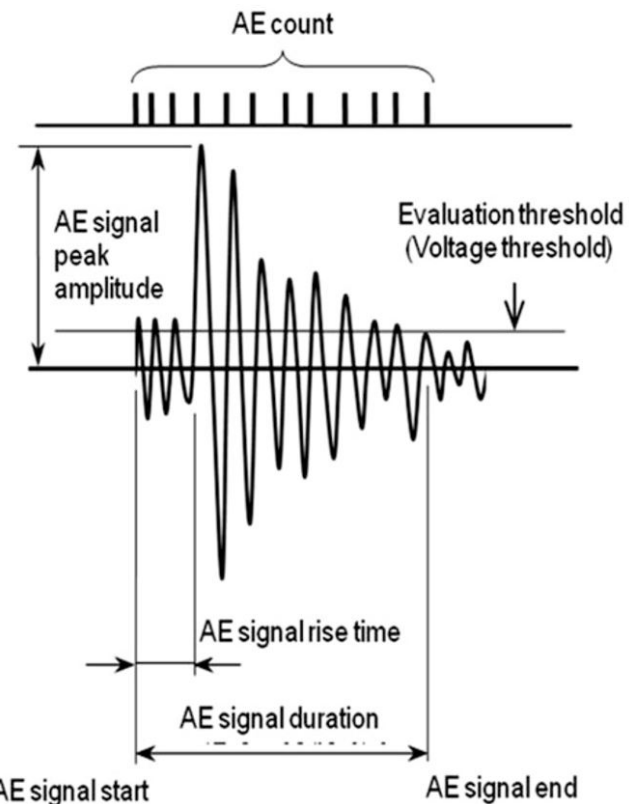


Figure 3.4 Time-domain AE signal feature [13]

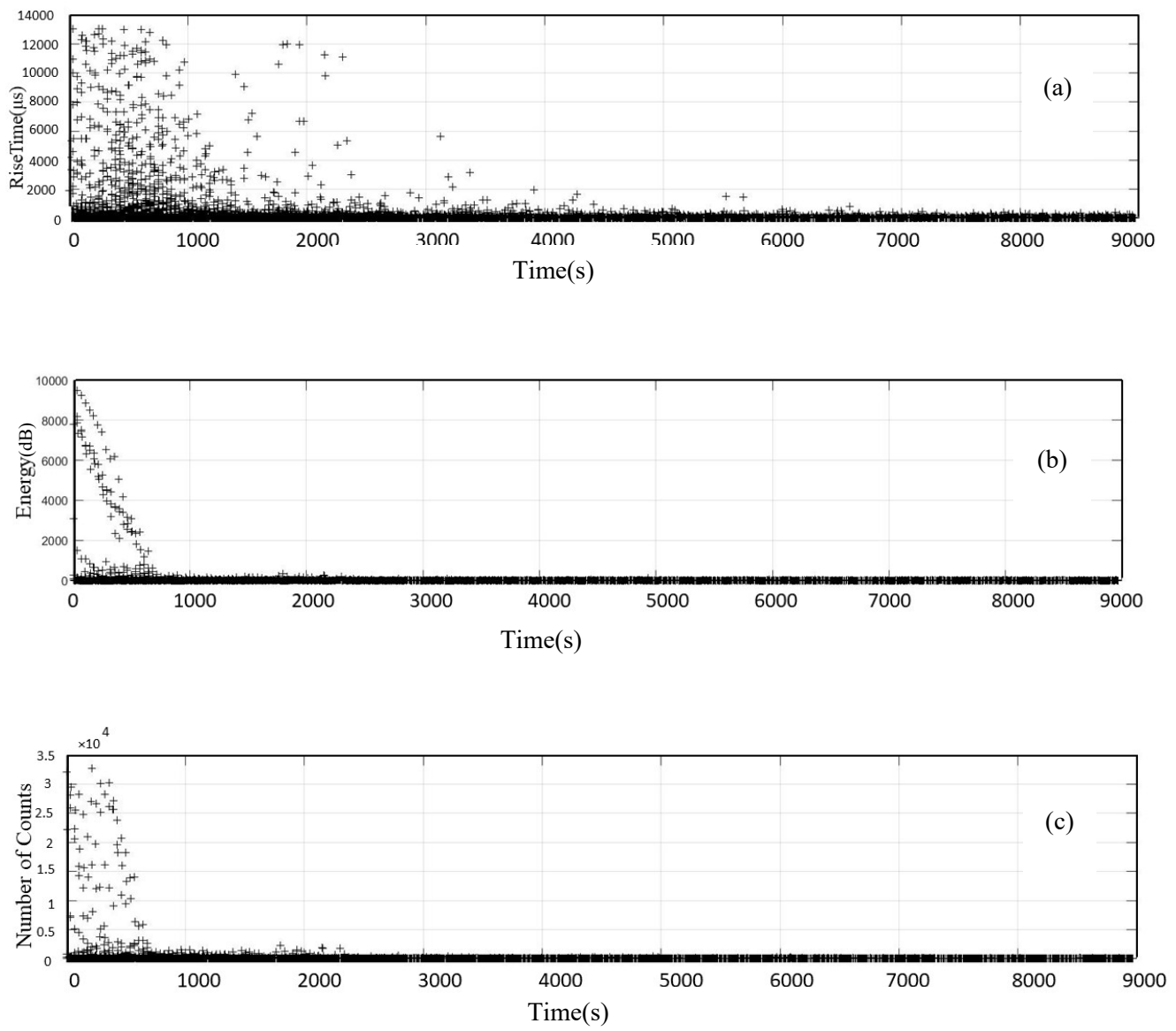


Figure 3.5(a) Rise time (b) Energy (c) Counts Vs Time for the whole process

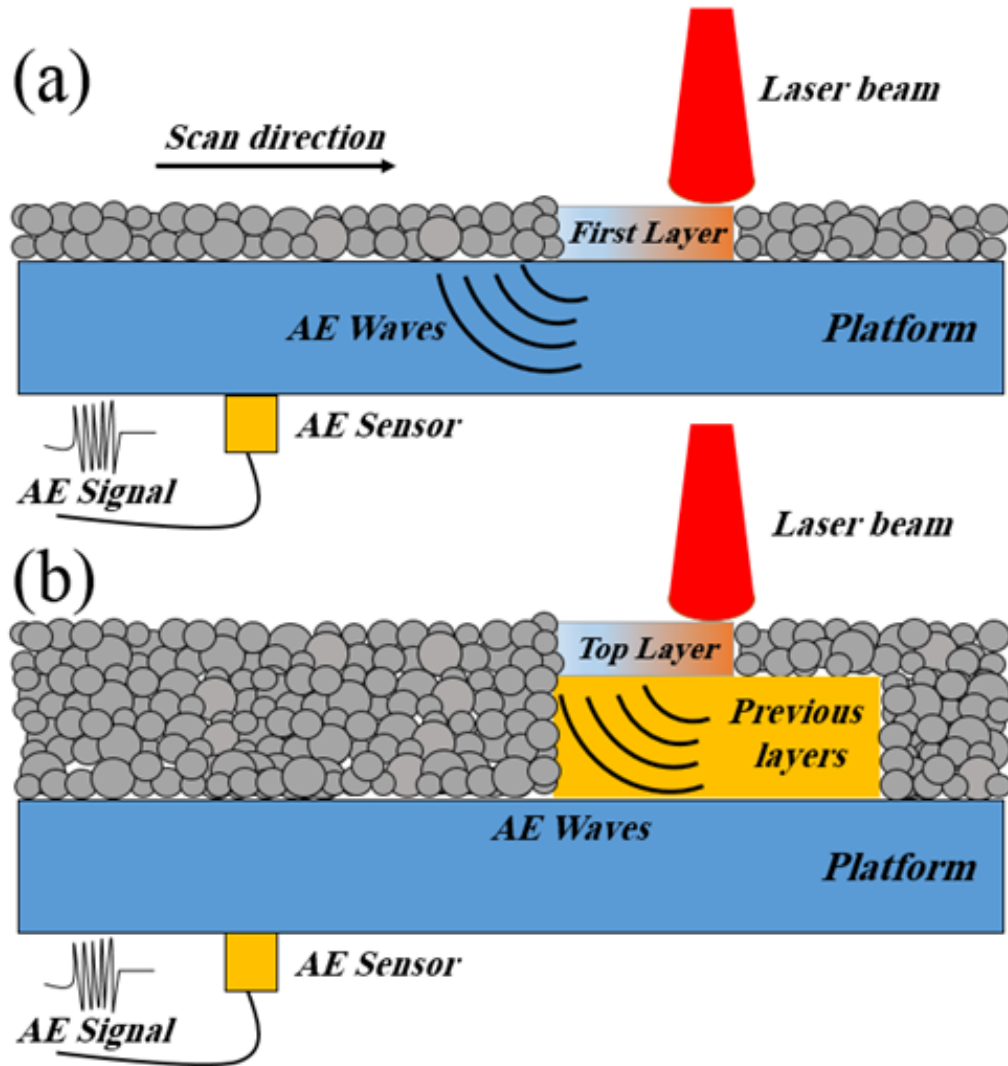


Figure 3.6. Schematic illustrations of the path that waves travel to reach the AE sensor in the case of (a) first layer, and (b) multiple layers.

### 3.3.2 Unsupervised results

Fast Fourier Transform (FFT) converts a signal from its original time-domain to the frequency-domain. Complex numbers are represented as  $X_0, \dots, X_{(N-1)}$ . The Discrete Fourier Transform (DFT) is defined by the following formula:

$$X_k = \sum_{n=0}^{N-1} x_n e^{-i2\pi kn/N} \quad k = 0, \dots, N-1 \quad 2.5$$

where the primitive Nth root of 1 is  $e^{i2\pi/N}$  [14].

Using FFT, all waveforms were transformed into the frequency-domain. Afterwards, all frequency results were clustered into four groups. The elbow method was used to find the optimum number of clusters, which [15].

In this clustering process, the entire frequency vector was used as the features of each sample. This is due to the fact that in most waveforms there are two or more dominant frequencies; therefore, using frequency peak can produce errors. From the mechanical perspective, having two dominant frequencies is reasonable since during solidification, defects such as cracks, porosities and more can make AE signals too.

In Figure 3.7, one example of the frequency-domain samples for each cluster is shown. Each cluster can be related to the produced parts based on the time of signals. Each cluster can be related to the quality of the samples based on their energy density and prior research [16]. The start time, end time, waveform and frequency-domain of each signal is available. Clustering of signals was on the frequency domain. Based on the recorded time of each signal, cluster No. 0 can be related to the effect of the recoating process in each layer. Cluster No. 1 can be related to samples with a high-quality, cluster No. 2 to samples with medium-quality, and cluster No.3 to samples with poor-quality [16].

Low-quality samples have micro-cracks, voids, and un-melted particles. Medium-quality ones show fewer voids and cracks and partially melted particles than low-quality samples. Lastly, high-quality samples have no voids or cracks and display a stable melting process, where the particles are fully melted. For this purpose, the number of cracks, porosities and density of each part help to assign parts to their groups. Figure 3.8 shows the top surface of low, medium, and high-quality parts.

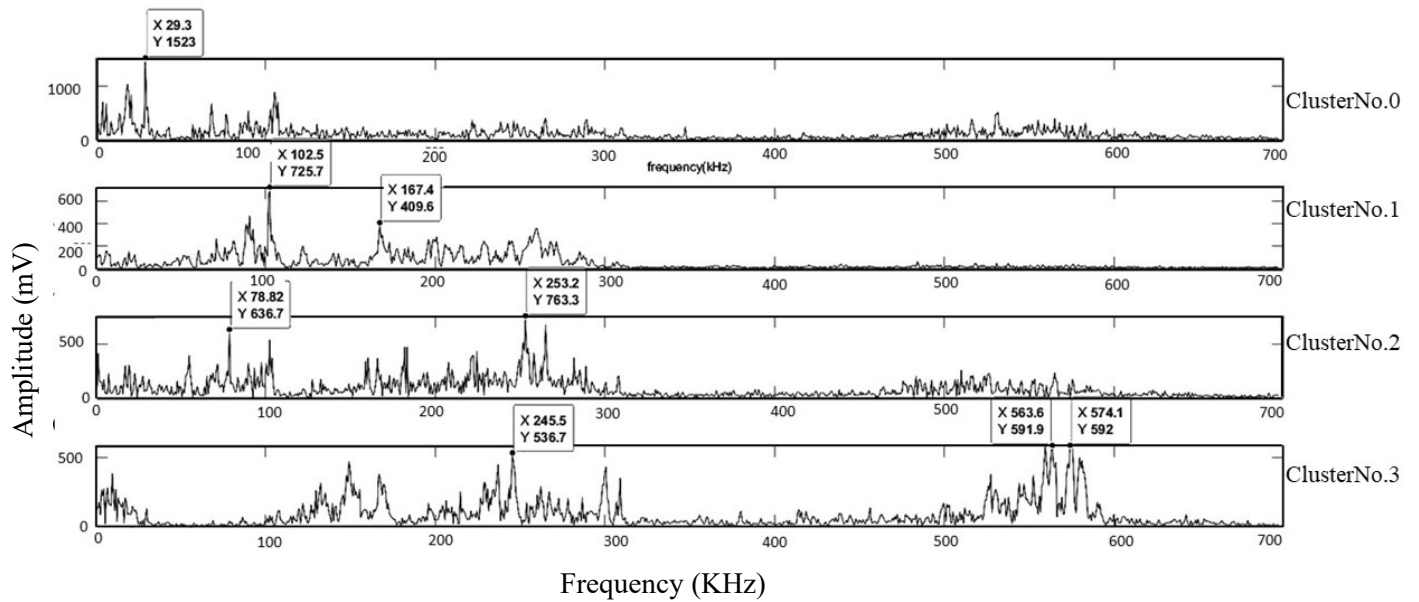


Figure 3.7 Cluster results in the frequency domain

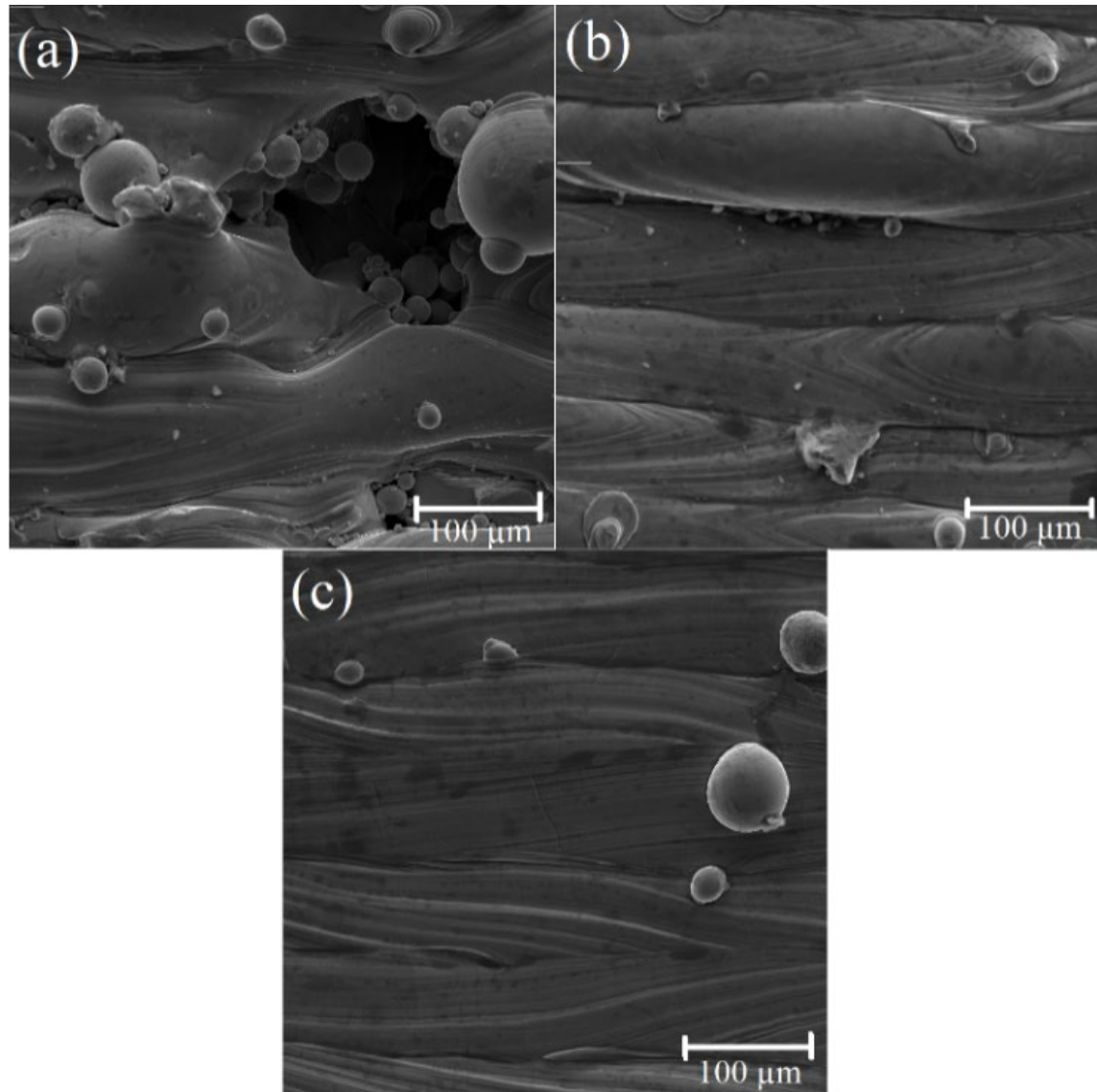


Figure 3.8 Microstructures of the top surfaces of samples  
with (a) low-quality (b) medium-quality and (c) high quality [16]

### 3.3.3 Supervised results

Each sample is labelled under one of three classes: poor, medium, and high quality. They were classified using the deep learning classifier and tested on 15% of the data set, which is the frequency-domain of all waveforms (transformed by FFT). The results are shown in Table 3-5 in the form of a confusion matrix. In order to evaluate the performance of a model, a confusion matrix is used. In this matrix, there are columns and rows which indicate the actual and predicted values of the data, respectively. If a diagonal matrix is achieved, the model works perfectly; otherwise, errors have been introduced to the model. To quantify the accuracy of the model in each class, the number in the diagonal position of that class is divided by its total value[17]. There are 91%, 77%, and 70.8% accuracy for class No. 1, No. 2, and No. 3, respectively. In total, an 85.9% accuracy level was observed. Also, it took 0.5087 seconds for one layer to be transformed from the time-domain waveform to frequency-domain and be classified via deep learning with a regular core i7 computer, all through the parallel process.

Class No. 1, representing the high-quality samples, has the least amount of errors in comparison to the other classes. Since the poor and medium quality samples have both defective layers and high-quality layers, these classes have more significant errors.

Table 3-5. Confusion Matrix.

		Actual value		
Classes Numbers		No.1	No.2	No.3
Predicted value	No.1	<b>1563</b>	73	35
	No.2	58	<b>403</b>	52
	No.3	93	46	<b>211</b>
	Total value of each class	1714	522	298

### **3.4 Conclusion**

In this study, real-time monitoring of L-PBF was investigated via a novel AE-based approach. FFT analysis was utilized to extract frequency-domain information. The frequency-time domain contained a vast array of processing information, such as pure consolidation, micro-cracks, and porosity. By using an unsupervised Machine learning method, the correlation between AE signals and processing information was determined. The deep learning method helps to create models which predict the quality of printed parts. Thus, AE can be a good output candidate for online monitoring systems in L-PBF processing.

### 3.5 References

1. Petrovic, V., et al., *Additive layered manufacturing: sectors of industrial application shown through case studies*. International Journal of Production Research, 2010. **49**(4): p. 1061-1079.
2. Leal, R., et al., *Additive manufacturing tooling for the automotive industry*. The International Journal of Advanced Manufacturing Technology, 2017. **92**(5-8): p. 1671-1676.
3. Everton, S.K., et al., *Review of in-situ process monitoring and in-situ metrology for metal additive manufacturing*. Materials & Design, 2016. **95**: p. 431-445.
4. Lu, Q.Y. and C.H. Wong, *Additive manufacturing process monitoring and control by non-destructive testing techniques: challenges and in-process monitoring*. Virtual and Physical Prototyping, 2017. **13**(2): p. 39-48.
5. Boyes, W., *Instrumentation reference book*. 2009: Butterworth-Heinemann.
6. Kruth, J.-P., et al., *Consolidation phenomena in laser and powder-bed based layered manufacturing*. CIRP annals, 2007. **56**(2): p. 730-759.
7. Ye, D., et al., *Characterization of acoustic signals during a direct metal laser sintering process*. 2017, Advances in energy science and equipment engineering II. CRC Press.
8. Shalev-Shwartz, S. and S. Ben-David, *Understanding machine learning: From theory to algorithms*. 2014: Cambridge university press.
9. Taheri, H., et al., *In Situ Additive Manufacturing Process Monitoring With an Acoustic Technique: Clustering Performance Evaluation Using K-Means Algorithm*. Journal of Manufacturing Science and Engineering, 2019. **141**(4).
10. Francois, C., *Deep learning with Python*. 2017, Manning Publications Company.
11. Loh, L.-E., et al., *Numerical investigation and an effective modelling on the Selective Laser Melting (SLM) process with aluminium alloy 6061*. International Journal of Heat and Mass Transfer, 2015. **80**: p. 288-300.
12. Spierings, A.B. and G. Levy. *Comparison of density of stainless steel 316L parts produced with selective laser melting using different powder grades*. in *Proceedings of the Annual International Solid Freeform Fabrication Symposium*. 2009. Austin, TX.
13. Ohtsu, M., et al., *Principles of the acoustic emission (AE) method and signal processing*, in *Practical acoustic emission Testing*. 2016, Springer. p. 5-34.
14. Oran Brigham, E., *The fast Fourier transform and its applications*. UK: Prentice Hall, 1988.
15. Kodinariya, T.M. and P.R. Makwana, *Review on determining number of Cluster in K-Means Clustering*. International Journal, 2013. **1**(6): p. 90-95.
16. Yakout, M., M. Elbestawi, and S.C. Veldhuis, *A study of thermal expansion coefficients and microstructure during selective laser melting of Invar 36 and stainless steel 316L*. Additive Manufacturing, 2018. **24**: p. 405-418.
17. Meyer-Baese, A. and V.J. Schmid, *Pattern recognition and signal analysis in medical imaging*. 2014: Elsevier.

## **Chapter 4**

### **On the application of machine learning for defect detection in L-PBF additive manufacturing**

#### **Complete Citation:**

Mohammadi, Mohammad Ghayoomi, Dalia Mahmoud, and Mohamed Elbestawi. "On the application of machine learning for defect detection in L-PBF additive manufacturing." *Optics & Laser Technology* 143 (2021): 107338.

**Abstract:**

This paper investigates the performance of several Machine Learning (ML) techniques for online defect detection in the Laser Powder Bed Fusion (L-PBF) process. The research aims to improve the consistency in product quality and process reliability. The applications of acoustic emission (AE) sensor to receive elastic waves during the printing process is a cost-effective way of materializing such a demand. In this study, the process parameters were intentionally adjusted to create three different levels of defects in H13 tool steel samples. The first class was printed with minimum defects, the second class had only intentional cracks, and the last class included both intentional cracks and porosities. The AE signals were acquired during the samples' manufacturing, and three different machine learning (ML) techniques were applied to analyze and interpret the dataset. First, a hierarchical K-means clustering is employed for labeling the data, followed by a supervised deep learning neural network (DL) to match acoustic signal with defect type. Second, a principal component analysis (PCA) was used to reduce the dimensionality of the dataset. A Gaussian Mixture Model (GMM) was then employed to enable fast defect detection suitable for online monitoring. Third, a variational auto-encoder (VAE) approach is used to obtain a general feature of the signal that could be an input for the classifier. A supervised DL trained on the H13 tool steel dataset successfully detected quality trends in AE signals collected from 316L samples. The VAE approach presents a novel method to detect defects in L-PBF processes that eliminate the need for model training in different materials.

**Keywords:**

Acoustic emission, Laser powder bed fusion, Deep learning neural network, K-means, Principal component analysis, Variational auto-encoder

**Highlights:**

- Presented a method in-situ monitoring the L-PBF process using AE signature.
- Classified defect types in L-PBF using a hierarchical K-means clustering approach.
- Demonstrated the effectiveness of PCA and GMM for anomaly detection.
- Developed a generalized machine learning model to classify defects without training.

## 4.1 Introduction

Additive Manufacturing (AM) has gained significant attention in the past two decades, where complicated parts can be built in a layer-by-layer manner. This is in contrast with the subtractive manufacturing techniques whereby the desired part is obtained by removing material [1]. AM has several advantages; for example, it offers nearly infinite freedom of design and can create complex geometries and lightweight parts created from lattice structures[2]. In addition, the AM process does not generate material waste and does not need part-specific tooling [3]. Powder bed fusion (PBF) is one type of AM processes that is capable of fabricating metallic components[4]. A mechanical re-coater is used to spread a layer of powder evenly, then a power source (laser or electron beam) is used to sinter/melt one layer of the part. Then the build platform is lowered, and the cycle is repeated [5].

Although AM technologies have already been utilized to manufacture end products, their full implementation across industries is hindered by structural defects developed during the process resulting in a lack of repeatability in the end products [6]. Experimental optimization of the process through the design of experiments is time-consuming and costly. Moreover, numerical optimization requires models to be applied on a multiscale level, hence, computationally expensive [7]. The need for higher quality assurance represents a significant technological barrier preventing AM from being adopted as a widespread manufacturing technique. There is a need to produce parts consistently, especially in safety-critical applications such as aerospace and medical industries [8, 9].

One way to achieve better consistent part production is to monitor the build process in real-time via sensors to control key process parameters via software use [10]. In this manner, if one of the

observed parameters deviates from its specified requirement, it can be adjusted to keep the build on track. The ability to adjust build parameters in an in-situ manner drastically increases efficiency, saves time, and reduces cost as the scrap rate declines [11]. However, currently, most of the sensor data processing occurs post-build, making the control impossible. Moreover, traditional offline testing is typically destructive and costly, leading to strong demand for in-situ monitoring and control [12].

There are many variables that affect the AM process, such as laser power, scanning speed, hatch spacing, layer thickness, and the type of inert gas. There are two main categories of imperfections that occur in AM: surface defects and internal defects [13]. Surface defects include roughness caused due to the selection of inappropriate process parameters and the staircase effect [14]. Internal defects include porosity and cracks due to the selection of inappropriate process parameters as well. In-situ monitoring processes need higher recognition accuracy, faster speeds, and less computational cost. Intelligent methods are widely used in defect detection and manufacturing process monitoring [15, 16]. Sensors used to detect these types of defects include pyrometers, CMOS cameras, High-speed cameras, Acoustic Emission (AE) sensors, and Infrared (IR) cameras[17, 18]. These can be either externally mounted on the build unit or mounted within the build chamber, although external mounting is often favored due to the harsh build environment [13].

AE sensors are considered an economical solution and have considerably easier installation compared to other in situ sensors. Applying artificial intelligence algorithms such as machine learning (ML) to AE signals is a common approach that is suitable for classifying wave sources. AE sensors quickly spot elastic waves and then convert them to transient electric waves and record

information during the process. Fracture, plastic deformation, and crack initiation and growth are some examples of this type of activity [19]. AE is a sensitive method, detecting 25  $\mu\text{m}$  crack growths compared to the 0.55 mm crack growths detected via ultrasound and radioactive testing[20]. Compared to other non-destructive test techniques, AE monitoring also identifies flaws developed during the process on much smaller scales [20]. AE setup benefits from ease of use in LPBF machines as it can be easily mounted under the subsurface of the build plate.

Several research groups have recently studied the application of ML techniques with AE signals in AM. For example, Wasmar et al. [21] used a convolution neural network to classify the AE wavelet-based features captured while manufacturing 316L samples to detect the printed parts' quality level. While Shevchik et al. [22] used Fast Fourier Transform (FFT) based features as an input to spectral convolutional neural networks to detect CL20ES stainless steel's quality level. Eschner et al. [23] used frequency domain AE input in an artificial neural network algorithm to classify the AE signature of 316L samples printed using the L-PBF process. Gaja et al. [24] implemented a defects monitoring system to detect and classify defects in real-time with the aid of an AE sensor and an unsupervised pattern recognition analysis (K-means clustering) along with a principal component analysis (PCA) for two defect types. It was noted that very few studies had covered the reduction of the AE signals dimensionality of the large dataset collected during the L-PBF process [24]. Moreover, most of the proposed algorithm is trained to detect defects in a single material, and the need to generalize the models to cover different materials is present.

The main contribution of this work is evaluating three ML techniques to detect the defects in H13 tool steel parts printed using the L-PBF process. The first algorithm utilizes a hierarchical K-mean approach for labeling data with a supervised deep learning neural network (DL) classifier to

enhance the classification accuracy. The second algorithm uses a principal component analysis (PCA) and anomaly detection technique to reduce the data dimension. By fitting the reduced data to a Gaussian Mixture Model (GMM), a fast detection method suitable for online monitoring and control systems of L-PBF processes was developed. Finally, a variation auto-encoder (VAE) was used for the AE signals as a feature extractor module. Then a DL classifier was used to generalize the detection method regardless of the material type. The classifier's accuracy was tested by AE signals acquired during the manufacturing of 316L stainless steel samples.

The article is structured as follows: first, the used AE signal processing and ML algorithm's theoretical background is described in section 2. The experimental work and signal acquisition is described in section 3. The results and discussion are provided in section 4, and section 5 is the conclusion and future recommendations.

## 4.2 Theoretical background

### 4.2.1 AE Signal Processing

Pre-processing of the AE signal is necessary to ensure effective analysis of the collected dataset. The first step usually includes removing noises from the raw data by wavelet denoising tools. The second step involves converting the waveform from a time-domain to a frequency-time domain using a Fast Fourier transform (FFT). Waveform describes the shape of a signal as a function of time which in Acoustic emission corresponds to the displacement of piezoelectric in the AE sensor in time. Hence, the waveform is a 1-D function of time[25]. Afterward, normalization of the AE signals is usually performed to ensure a consistent comparison between different signals acquired at different locations and parts.

#### 4.2.1.1 Fast Fourier Transform

Using frequency-domain features achieved higher accuracy than raw signals [26] and wavelet-based features [22]. FFT converts signals from their original time to the frequency domain. Using FFT helps to analyze a time-dependent phenomenon and for AE signals waveforms. Complex numbers are represented as  $x_0, x_1, \dots, x_{N-1}$ . The Discrete Fourier Transform (DFT) is defined as follows:

$$X_k = \sum_{n=0}^{N-1} x_n e^{-i2\pi kn/N} \quad k = 0, \dots, N-1 \quad 4.1$$

The primitive  $N^{\text{th}}$  root of 1 is  $e^{i2\pi/N}$ [27].

#### 4.2.1.2 Discrete Cosine Transform (DCT)

Using the DCT and the Inverse DCT (IDCT) helped accomplish a very low loss value and improved the DL classification accuracy. A discrete cosine transform (DCT) is widely used in signal processing and data compression when transformation techniques are required. The most important feature of the DCT method is that it is insensitive to noise, and the amplitude detection is not influenced by mutation[28]. Also, DCT is a Fourier-related transform similar to the discrete Fourier transform (DFT) but using only real numbers. DCT displays a finite sequence of data points as a sum of cosine functions oscillating at different frequencies and is often used in digital media, including speech coding.

The discrete cosine transform is a linear, invertible function.

$$f: \mathbb{R}^N \rightarrow \mathbb{R}^N$$

Where  $\mathbb{R}$  symbolizes a set of real numbers.

There can be eight types of DCT. "DCT" usually refers to DCT type 2, and "IDCT (known as Inverse DCT)" typically refers to DCT type 3.  $N$ , real numbers  $x_0, \dots, x_{N-1}$  are transformed into the real numbers  $X_0, \dots, X_{N-1}$ , which are known as frequency coefficients.

DCT-II:

$$X_k = \sum_{n=0}^{N-1} x_n \cos\left[\frac{\pi}{N}\left(n + \frac{1}{2}\right)k\right] \quad k = 0, \dots, N-1 \quad 4.2$$

Some researchers further multiply the  $X_0$  term by  $1/\sqrt{2}$  and then multiply the  $X$  vector by a scale factor of  $\sqrt{2/N}$ . This process makes the DCT-II frequency coefficients orthogonal. In

"information compression", cosine is used instead of sine functions as fewer cosine functions are required to approximate a typical signal.

#### **4.2.2 Machine learning algorithms:**

This section discusses the theoretical background of the different ML techniques used in this work.

##### *4.2.2.1 K-Means Clustering Algorithm*

Clustering is among the most conventional methods for exploratory data analysis [29]. The K-means algorithm is an efficient classifier for data points with a predefined number of clusters. Also, it goes through large amounts of data quickly and helps to produce a meaningful intuition of the data structure. The K-means objective function is a popular clustering analysis within data mining. K-means clustering is a vector quantization method drawn from signal processing. In the K-means algorithm, data is segregated into disjoint sets  $C_1, \dots, C_k$  where a centroid denotes each  $\mu_i$ . Partitioning  $n$  observations into K clusters. Thus, each observation fits into the cluster with the closest mean. The purpose is to create a cluster prototype so that the data space is partitioned. K-means minimizes variances in each cluster, which is represented as squared Euclidean distances. The assumption is that the input set is embedded within some large metric space  $(X', d)$  (so that  $X \subseteq X'$ ), and the centroids are members of  $X'$ . The K-means measures the squared distance between the centroid of the cluster and each point in  $X$ . The centroid  $C_i$  is defined as:

$$\mu_i(C_i) = \arg \min_{\substack{x \in C_i \\ \mu \in X'}} \sum_{x \in C_i} d(x, \mu)^2 \quad 4.3$$

The k-means objective is defined as:

$$G_{k-means}((X, d), (C_1, \dots, C_k)) = \sum_{i=1}^k \sum_{x \in C_i} d(x, \mu_i(C_i))^2 \quad 4.4$$

which can also be rewritten as the following:

$$G_{k-means}((X, d), (C_1, \dots, C_k)) = \min_{\mu_1, \dots, \mu_k \in X} \sum_{i=1}^k \sum_{x \in C_i} d(x, \mu_i)^2 \quad 4.5$$

#### 4.2.2.2 PCA- GMM

Gaussian Mixture Models (GMM) are a time-efficient approach to classify data since they use expectation-maximization algorithms [30]. GMM algorithm is built with the gaussian probability distribution (normal distribution) to quantify data and decompose it into several parts based on the Gaussian probability distribution. In the case of AE signals, the data dimension is large; it might become difficult or even impossible to apply GMM [31]. The reduction in data dimensions can be obtained through applying the principal component analysis (PCA) algorithm. The most important feature about the PCA application is that the inevitable loss of data information is prevented [32].

Assume that we are given a  $n \times m$  data matrix, where X has n samples of m-dimension vectors  $\vec{x}_i \in \mathbb{R}^m$ . First, the mean and covariance of the data matrix are computed. X's covariance matrix is  $S \in \mathbb{R}^{m \times m}$  and is defined by:

$$\Sigma = \frac{1}{n} \sum_{i=1}^n (\vec{x}_i - \bar{\vec{x}})(\vec{x}_i - \bar{\vec{x}})^T \quad 4.6$$

where  $\bar{\vec{x}}_i \in \mathbb{R}^m$  is the mean of each row in X and is defined by:

$$\bar{x} = \frac{1}{n} \sum_{i=1}^n \vec{x}_i \quad 4.7$$

Then the singular vector decomposition (SVD) of  $S$  is used to extract principal components and directions via the following equation:

$$S = U \Sigma V^T \quad 4.8$$

where  $U \in \mathbb{R}^{n \times n}, \Sigma \in \mathbb{R}^{n \times m}, V \in \mathbb{R}^{m \times m}$

In the implementation process, the matrix  $V = [u_1 u_2 \dots u_m]$  was used, where the vector  $u_i \in \mathbb{R}^m$  represents a primary component direction.

Afterward, the data matrix  $X$  can be projected into  $Y \in \mathbb{R}^{k \times m}$  a new matrix by multiplying a matrix  $P^T$

$$Y = P^T X \quad 4.9$$

where  $P = [u_1 u_2 \dots u_k], k \leq m$ . The proper number of principal components  $k$  is selected before the projection of the data matrix.

Anomaly detection algorithms are beneficial within manufacturing and industry settings as they aid in catching potentially severe problems at early stages. Manufacturing organizations have used statistical change detection algorithms for quality control for a long time. When the quality of sampled output characteristics of a product falls below expected constraints, alarms are triggered. Generally, fluctuations in the underlying process are detected by drastic changes within specific sensor data measurements. These algorithms are known as simple anomaly detection algorithms.

Moreover, anomaly detection applies to data from various sensors located at multiple points in the monitored manufacturing environment. Anomalies can be detected after they have occurred and when unusual patterns of various sensor data occur, which indicates the location of possible faults or failures in the manufacturing environment. For example, suppose the "normal" behavior of two adjacent sensors depicts a linear relationship over time. In that case, a significant variation in this relationship is marked as an anomaly and triggers further investigation.

The simplest anomaly detection algorithms are based on data distribution assumptions; here, data is two-dimensional and normally distributed with a mean of  $\mu$  and standard deviation of  $\Sigma$ . A large distance from the center of the distribution implies a low probability of observing such a data point. As there is only a low probability of observing a data point far away from the center, it would be labeled an anomaly[33]. The occurrence probability of each data is as follow:

$$p(x; \mu, \Sigma) = \frac{1}{(2\pi)^{\frac{m}{2}} |\Sigma|^{\frac{1}{2}}} \exp(-\frac{1}{2}(x - \mu)^T \Sigma^{-1} (x - \mu)) \quad 4.10$$

Given a training set of  $X$ ,  $\mu$  and  $\Sigma$  are as the following:

$$\mu = \frac{1}{n} \sum_{i=1}^n x^{(i)} \quad 4.11$$

$$\Sigma = \frac{1}{n} \sum_{i=1}^n (x^{(i)} - \mu)(x^{(i)} - \mu)^T \quad 4.12$$

#### 4.2.2.3 Variational Auto Encoders (VAE)

Variational Autoencoders (VAEs) are autoencoder-based machine learning algorithms. This neural network architecture finds structure in input data to represent it in a compressed form. Autoencoders are predominantly made of an encoder, decoder, and loss function [34]. The encoder is a symmetric neural network that converts information from an input sample into a vector. The encoder takes the high-dimensional data ' $x$ ' and converts it to the lower representational space ' $z$ ', including weights and biases. This conversion process is called a bottleneck. The encoder's goal is to compress data into lower-dimensional space efficiently. The decoder is another neural network that expands the vector to reconstruct the sample input into an output. The loss function measures the amount of data lost during the compression and reconstruction process and, through training, seeks to minimize loss [34]. A normal auto-encoder's main goal is to learn an input's hidden representation, transform an input into a vector, and minimize reconstruction loss occurring during training.

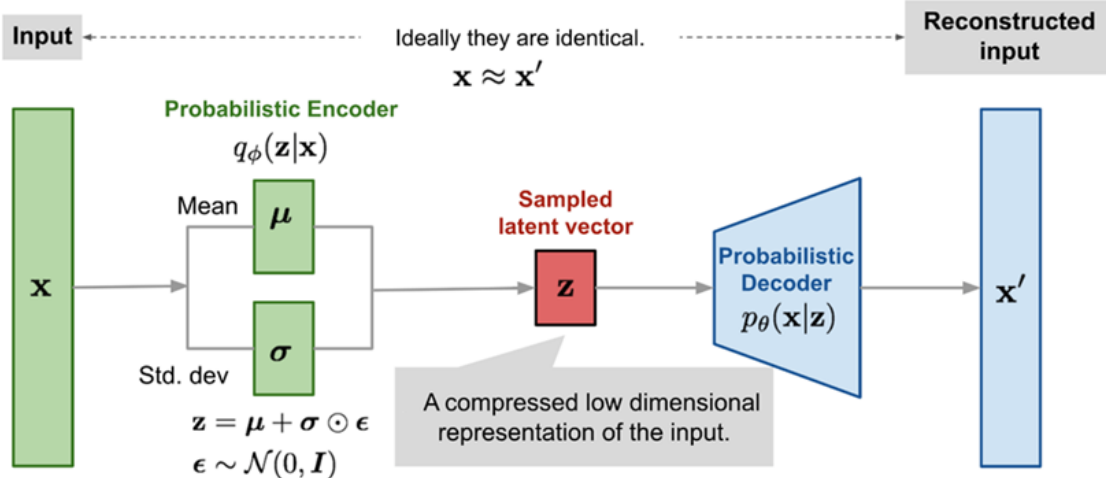


Figure 4.1VAE architecture with more details illustrated [35]

Let  $x$  denote the observation and  $z$  represent the latent variable in the following descriptions.

#### *4.2.2.3.1 Encoder (Inference) Network:*

This is an approximate posterior distribution  $q(z|x)$  that takes an observation as input and puts out latent representation's set of parameters for the conditional distribution. We can model the distribution as a diagonal Gaussian if the problems are mild or if the datasets are unchallenging. In this instance, the mean and log-variance parameters of a factorized Gaussian are put out by the inference network. Log-variance is used instead of directly using the variance for numerical stability.

#### *4.2.2.3.2 Decoder (Generative) Network:*

The input and output for the generative model are the latent encoding and parameters for a conditional distribution of observations, i.e.,  $p(x|z)$ , respectively. The latent variable used in this study was a unit Gaussian prior  $p(z)$ .

#### *4.2.2.3.3 Re-parameterization:*

During the optimization process, we can get a sample of  $q(z|x)$  from a unit Gaussian, multiply it by the standard deviation, and then add the mean. This ensures that the gradients pass to the inference network parameters through the sample. This is represented in Figure1.

#### *4.2.2.3.4 Loss function:*

Two loss functions can be used to train the model's parameters: a reconstruction loss forcing the decoded samples to match the initial inputs and the "KL divergence" (distribution loss) between the learned latent distribution and the prior distribution, acting as a regularization term. The "KL divergence" can often be neglected, although it reduces overfitting to the training data and helps learn well-formed latent spaces and. The concept of "KL divergence" comes originally from

information theory and describes the relative entropy between two probability distributions, "p" and "q." The "KL divergence" is often conceptualized as measuring some distance between these distributions. Minimizing the KL divergence means making the output distribution of the VAE sample similar to the input distribution, making VAE desirable property when applied in ML models [35].

$$D_{KL}(P||Q) = - \sum_{x \in X} P(x) \log\left(\frac{Q(x)}{P(x)}\right) \quad 4.13$$

The reconstruction loss used in this study is the Mean Squared Error (MSE), as defined by the following formula:

$$MSE = \frac{\sum_{i=1}^n (y_i - \hat{y}_i)^2}{n} \quad 4.14$$

#### 4.2.2.4 Deep learning for classification (DL)

The DL neural network is a family of ML algorithms that uses multiple processing layers to identify complex data features, which is very useful in complex tasks such as audio signal processing [36]. The main advantage of DL models is the combination of high accuracy and fast response time to detect defects[37]. Layers, input data, loss functions, and optimizers are components of neural network training. The layers form the network, and the input data targets the network, which consists of chained layers to map the input data into predictions. The loss function compares predictions to the targets and produces a loss value. This value measures how well predictions match expectations. Lastly, the optimizer updates the network's weights using the loss value.

An epoch is the number of times that all training vectors are used to update the weights. During batch training, all samples simultaneously go through the learning algorithm in one epoch before weights are updated. During sequential training, weights are updated after each vector's sequential passing through the training algorithm[38].

The model used had five layers; all were fully connected. The loss function chosen to train the model was categorical cross-entropy, and the optimizer chosen was Adam. Categorical cross-entropy for K class and n samples is calculated as follows:

$$L(y_{true}, y_{predict}) = \sum_i^n \sum_k^K -y_{true}^{(k)} \log(y_{predict}^{(k)}) \quad 4.15$$

### 4.3 Experimental setup:

#### 4.3.1 L-PBF processing

A 400 W laser-equipped OmniSint-160 LPBF machine was employed to produce the test samples. First, gas-atomized AISI H13 tool steel powder with a particle size range of 25–45  $\mu\text{m}$ . The powder's particle size distribution (PSD) was measured using a Malvern Master sizer 3000 device through the laser diffraction method. Although the individual process parameters have proven to be influential in the parts' final quality, the literature is replete with a close correlation between defects and volumetric energy density. This work aims to get predefined defects (based on the literature) and detect them upon application of ML. Hence, the influence of individual process parameters is not the focus of this work.

In this study, the layer thickness, hatch spacing, and scanning speed were set at 0.04 mm, 0.08 mm, and 300 mm/sec, respectively, for all samples. The laser power and volumetric energy density of each sample have been provided in

Table 4-1. Eight cylindrical parts with a 10 mm radius and 10 mm height (Figure 3) were produced in each run. In this study, three intentional classes were chosen based on previous work related to the process-structure-property of H13 tool steel[39]. The three classes used in this study for labeling were parts with minimum defects (class1), parts with cracks only (class2), and parts with both cracks and porosities (class 3). The adjusted process parameters to obtain these intentional defects are presented in Table 4-2. Figure 4.2 shows how the parts are printed on the build plate and the AE sensor's position.

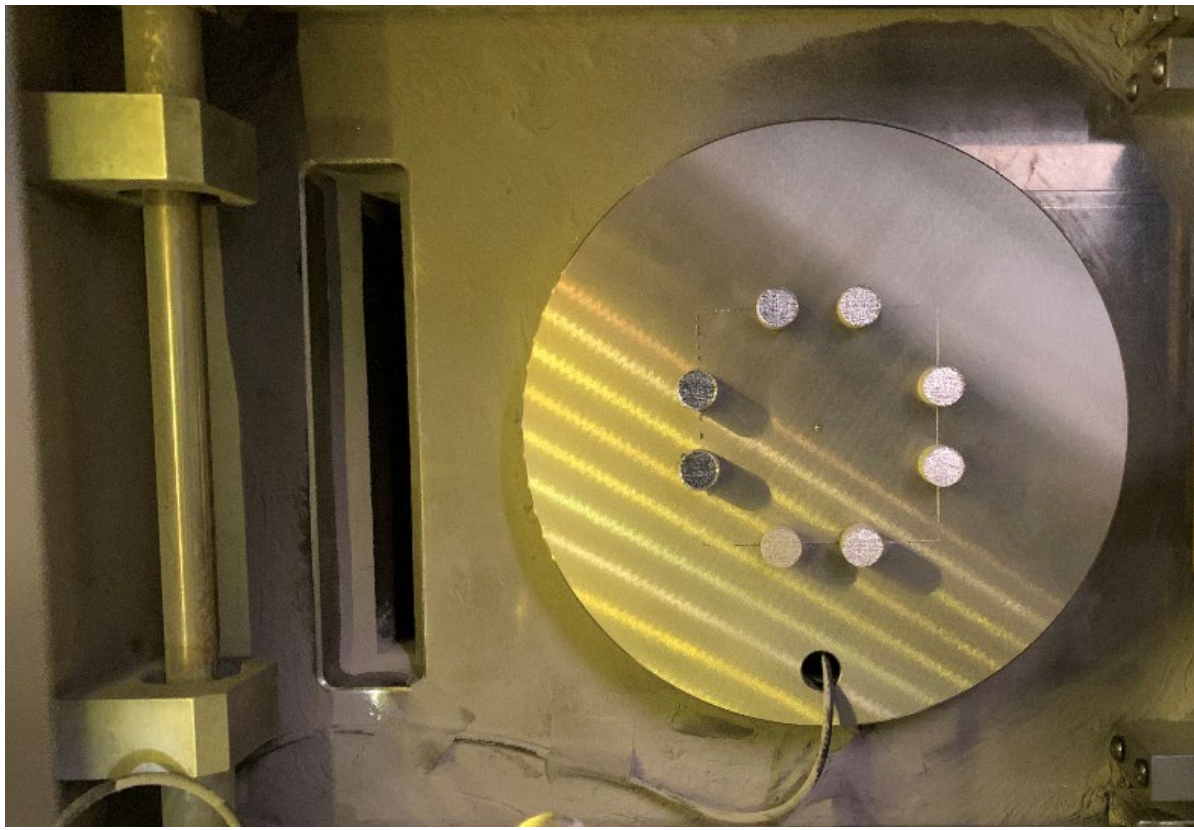


Figure 4.2. The process chamber showing the cylindrical samples printed on the build plate

Table 4-1: Parameters for H13 Tools Steel test experiments

Sample No.	Laser Power (W)	Energy Density (J/mm <sup>3</sup> )
1	100	104.1
2	200	208.3
3	225	234.3
4	275	286.4
5	300	312.5
6	325	338.5
7	350	364.0
8	375	390.6

Table 4-2: Different defect classes used for labelling the classifiers.

Defect Class	Description	Laser Power (W)	Energy density (J/mm <sup>3</sup> )
1	Minimum defects	375	390.625
2	Cracks only	350	364.583
3	Cracks and porosities	300	312.5

In the second experiment, gas-atomized stainless steel 316L powder was used to print eight cylindrical parts of a 10 mm radius and 10 mm height. The data collected from these parts were analyzed in our previous publication, and the raw AE signals were classified using the DL approach [40]. The layer thickness was set at 0.04 mm/sec, the hatch spacing at 0.08 mm/sec, and the scanning speed at 600 mm/sec. Table 4-2 contains the laser power and volumetric energy density of each sample; for both prints, samples were directly fabricated on the build plate without supports and no additional post-processing. The printed cylinders were removed using wire-cut Electrical Discharge Machining (EDM).

Table 4-3: Parameters for stainless steel 316L test experiments

Sample No.	Laser Power (W)	Energy Density (J/mm <sup>3</sup> )
1	75	39.0
2	100	52.0
3	150	78.1
4	180	93.7
5	200	104.1
6	220	114.5
7	250	130.2
8	300	156.2

### 4.3.2 AE system

The AE sensor used in this experiment was single-ended, wideband frequency WS<sub>0</sub>. This 100-900 kHz wideband frequency sensor was connected to a USB-AE node. The USB-AE-Node is a single channel Acoustic Emission (AE) Digital Signal Processor with full AE hit- and time-based features, entailing waveforms. With the aid of the USB Connector, the AE Node is readily interfaced to a Notebook or PC. The USB AE nodes could be connected to the available USB ports of a notebook. The AE Node can accept single-ended or differential sensors amplified by an internal low noise preamplifier. The sensor was attached to the build plate's center and bottom to detect the structure-borne acoustic emissions. The build plate was drilled to connect the sensor to

the PC, and the wire was transferred. To keep an equal distance between parts and the sensor, all parts were placed in a circular 4 cm radius. Before each test, the pencil lead break method was used according to the ASTM E976-15 standard to determine the AE sensor's reproducibility. The contact surface between specimens and the sensor was covered with vacuum grease to produce proper acoustical coupling.

To easily distinguish each layer from each part's wave, a time gap was allowed for melting each part in each layer. The time gap is left between each part and the others to allow a gap in the AE data collection to help separate between a part and the others. In other words, the gap may be regarded as another part being melted with a laser power of zero. Since the time allocated for the gap is relatively small (1.5 s), it is not expected to influence on the part's thermal behavior. The threshold parameter for the recorded data was 40 dB, with analog filtering of 20KHz as the lower bound and 1MHz as the upper bound. The sample rate was 1MSPS, and the pre-trigger was 16.00. The pre-Trigger value determines how long to record the wave until a specific threshold. Since the nature of the collected waves in this study is “burst,” a threshold of 16  $\mu$ s was set to capture the high importance data only.

The first step for AE signal processing was removing noises from the raw data by wavelet denoising tool in MATLAB toolbox. The second step was to convert the waveform from a time-domain to a frequency-time domain using a Fast Fourier transform (FFT). Fast Fourier Transform (FFT) signals were used to transform the AE signal as an input in the K-means and the GMM. Using frequency-domain features achieved higher accuracy than raw signals and wavelet-based features. Afterward, normalization of the AE signals was performed to ensure a consistent comparison between different signals acquired at different locations and parts.

## 4.4 Results and discussion:

### 4.4.1 K-Means Hierarchical Clustering for labeling

In this study, the K-means algorithm was used because it is an efficient classifier for data points with a predefined number of clusters. Also, it goes through large amounts of data quickly and helps to produce a meaningful intuition of the data structure. The role of the hierachal K-means algorithm in this research is to reduce the DL neural network's computational intensity. A downside of applying DL techniques for AM quality detection is the high amount of training needed and the large amount of noise collected with the data [37]. Therefore, by clustering the input, only selected samples from the clustered data schema will be used in the learning process. Resulting in reducing the number of samples used, the training time, and the required space while maintaining the important information due to its specific distribution.

Phase transformation, crack propagation, residual stresses, porosity formation, melting, and solidifying metal powders can all produce AE signals [3, 24, 41]. This work assumed all factors to be constant and considered only porosity and cracks as variables. Optical microscopy was used to examine the three different types of intentional defects in the printed H13 tool parts were observed, as shown in Figure 4.3 The FFT was then applied to all the collected signals were then processed as described in section 3.1.1.

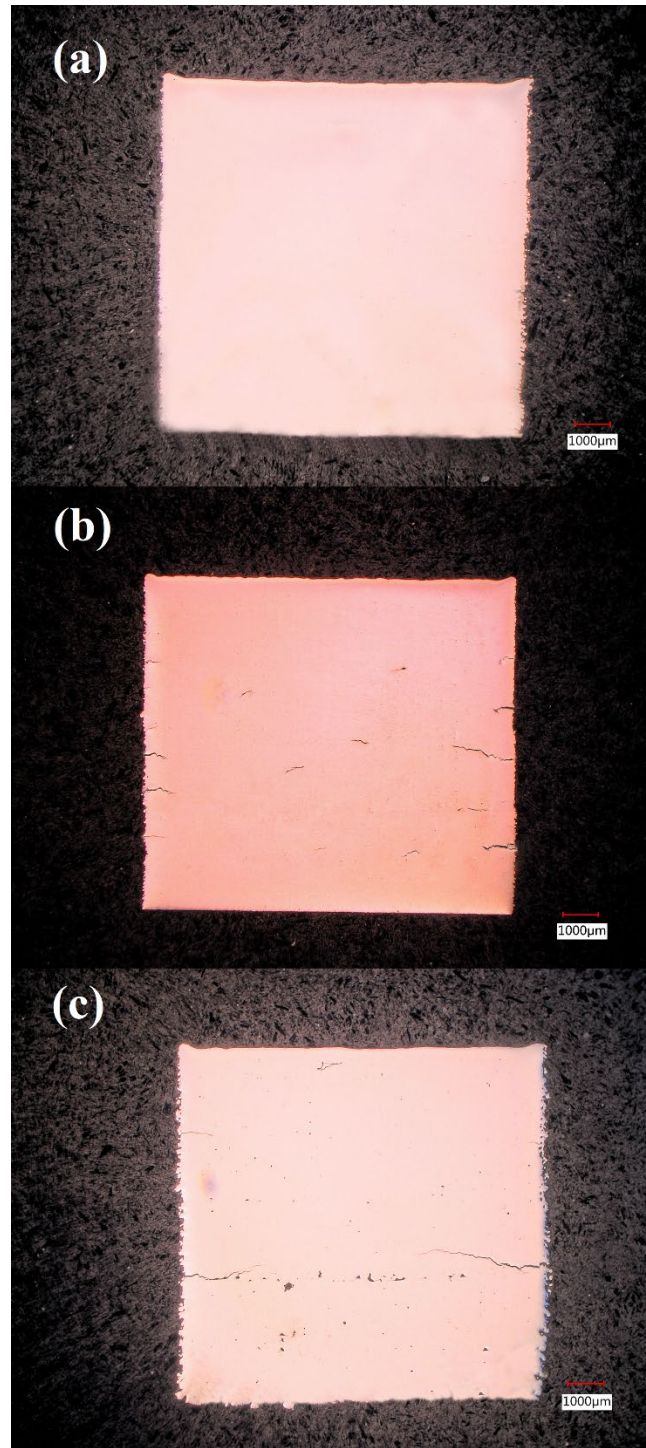


Figure 4.3: The cross-section of the samples along the build height with (a) no defects (class 1), (b) cracks only (class 2), and (c) both cracks and porosities (class 3).

Figure 4.4 describes the hierarchical K-means approach that was used to separate data based on the intentional defects of the H13 dataset. The first category presents AE signals related to the reference signal, regardless of the number of clusters the signal contains. The second category includes signals coming from parts with cracks only. This category has clusters with centers close to the previous one's centers and unique clusters representing cracks. The last category has clusters representing signals resulting from parts with porosities and cracks; the new unique clusters of the last dataset represent porosities. The optimum number of clusters for each data set is obtained by the Elbow method. The elbow method is used in cluster analysis to determine the number of clusters in a data set. The method plots the explained variation as a function of the number of clusters present and picks the elbow of the curve as the number of clusters to use [42].

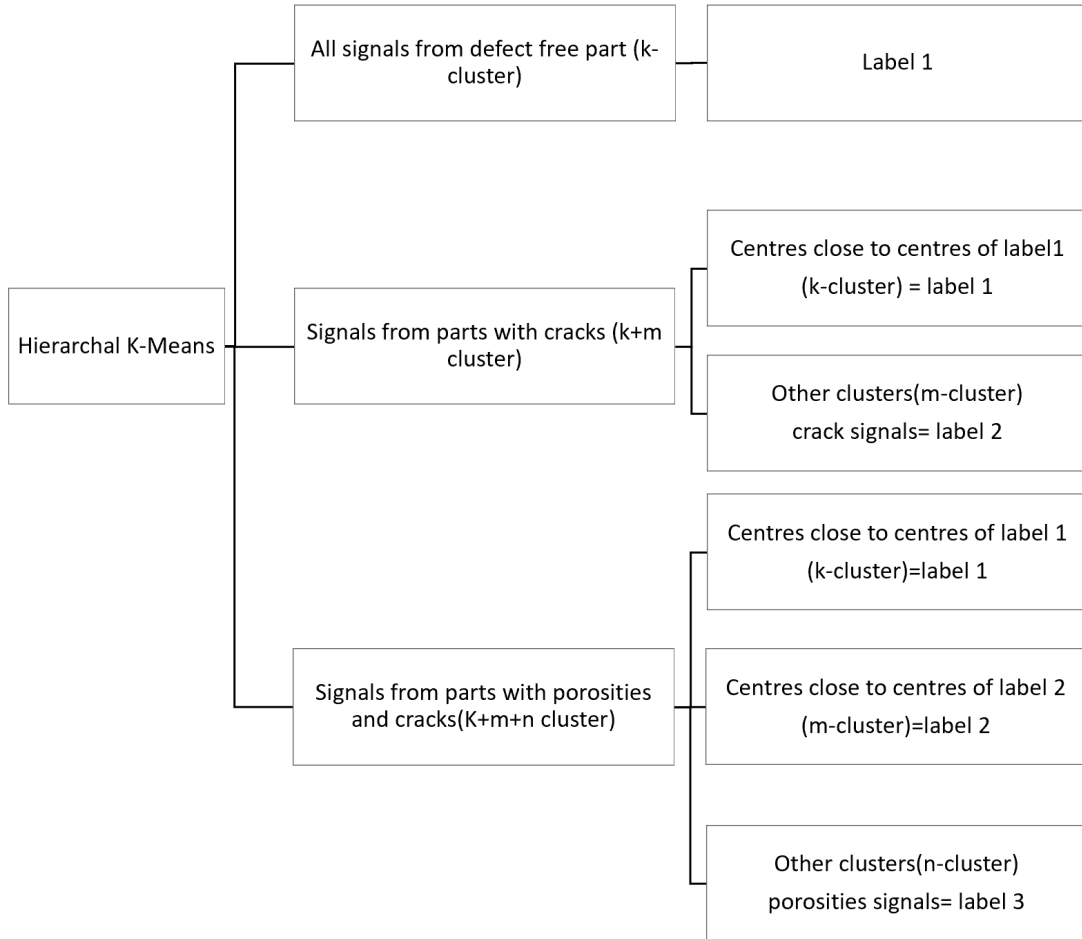


Figure 4.4: Schematic of the Hierarchal K-Means method

The three frequency-domain signals related to each type of defect are shown in Figure 4.5. Each frequency-domain signal has different features; afterward, the hierachal K means will be applied to cluster and label them.

#### 4.4.2 Deep Learning Classifier

Each sample is labeled under one of three classes: minimum defect parts without any cracks and porosities, parts with only cracks, and parts with cracks and porosities. Waveforms transformed in frequency-domain and were used as input for the hierarchical K-Means method. Afterward, all data were classified using a DL classifier as described in section 3.2.1. 60 % of the data was used for training and 15% validation and tested on 15% of the data set. The DL classifier had five layers; more details about the DL model can be found in our previous publication[40]. The results are shown in Table 4-4 in the form of a confusion matrix, and in

Table 4-5, the precision, recall, and F1 score are presented. A confusion matrix is used to evaluate the performance of a model in terms of accuracy. The columns and rows in this matrix indicate the actual and predicted values of the data, respectively. The model works perfectly If a diagonal matrix is achieved; otherwise, errors have been introduced to the model.

The number in each class's diagonal position is divided by its total value to quantify the model's accuracy in each class [43]. The accuracy of classes 1, 2, and 3 corresponded to 93.28%, 95.29%, and 97.30%. In total, a 94.56% accuracy level was achieved. Also, it took 0.4087 seconds for one AE signal to be transformed from the time-domain waveform to frequency-domain and be classified via DL with a regular core i7 computer. Class 1, representing the reference signal (AE signals coming from parts with minimum defects), has the highest classification errors compared to the other classes. Since the data in this class is the most common in the other categories as explained by the hierachal K-means. Class 2 and Class 3 present the signal originating from porosities and cracks, respectively. The high accuracy of Class 3 may be attributed to the unique signals coming from the porosities in these parts.

From Table 5, it can be seen that the highest precision value calculated was for class 1, meaning that the model is more accurate in predicting the minimum defect AE signals than AE signals coming from cracks and porosities. The highest recall value was found for class 3, attributed to AE signals related to the porosities, meaning that there is a small percentage of false negatives in this category. That is something preferable in the case of defect detection. In general, the high F1 score for all 3 cases indicates that the developed model is suitable for the application.

Table 4-4: The confusion Matrix of using DL model

Actual Values		Class 1	Class 2	Class 3
Predicted Values				
Class 1	<b>10073</b>	217	35	
Class 2	479	<b>8278</b>	40	
Class 3	246	192	<b>2703</b>	
Total number of data of each class	10798	8687	2778	
Accuracy percentage of each class	<b>93.2858</b>	<b>95.2918</b>	<b>97.3002</b>	

Table 4-5: Performance parameters used to classify the defect types.

Class Number	Precision	Recall	F1-score
1	0.975593	0.932858	0.953747
2	0.941003	0.952918	0.946923
3	0.860554	0.973002	0.91333

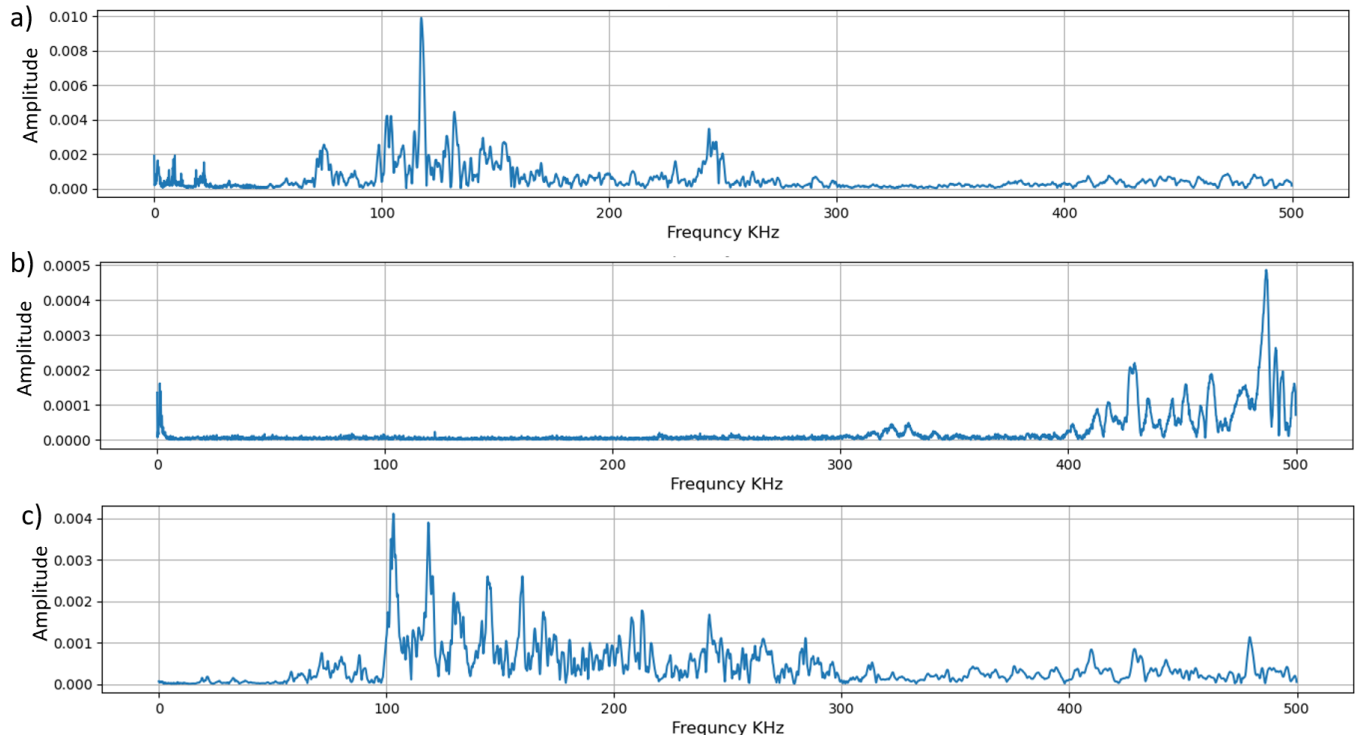


Figure 4.5: Frequency spectrum of H13 samples with intentional defects (a) minimum defects (class 1), (b) cracks only (class 2), and (c) porosities (class 3).

#### 4.4.3 PCA-GMM

In this study, PCA was used to reduce the waveform dimension to a 2D dataset and fitted using GMM as described in section 3.2.2. The number of AE signals related to defects can be considered a small portion of the total number of acoustic signals acquired within the L-PBF process. Therefore, there is a good potential for anomaly detection based on the normal gaussian model. Figure 4.6 illustrates how the data in 2D space after PCA was applied and how the Gaussian model fits into it. After reducing dimension to 2D, the mean-variance and the epsilon value (the threshold to show if it is anomalist or not) for 2D data is as follows:

$$\mu = [2.068 \times 10^{-16}, 1.65 \times 10^{-17}]$$

$$\Sigma = [0.0050, 2.5447 \times 10^{-4}]$$

$$\varepsilon = [0.4, 0.4]$$

An example data located in the outermost circle was chosen to show the effectiveness of this model. Figure 4.7 shows the waveform of this example data. Example data gaussian probability [0.3976, 0.3984] is less than  $\varepsilon$ , so it would be viewed as an anomaly in the model, as observed in Figure 4.7. By checking this example data using the developed DL classifier, it was classified as a crack signal. This example demonstrates the anomaly detection model's efficiency in detecting the cracks and porosities from large data sets.

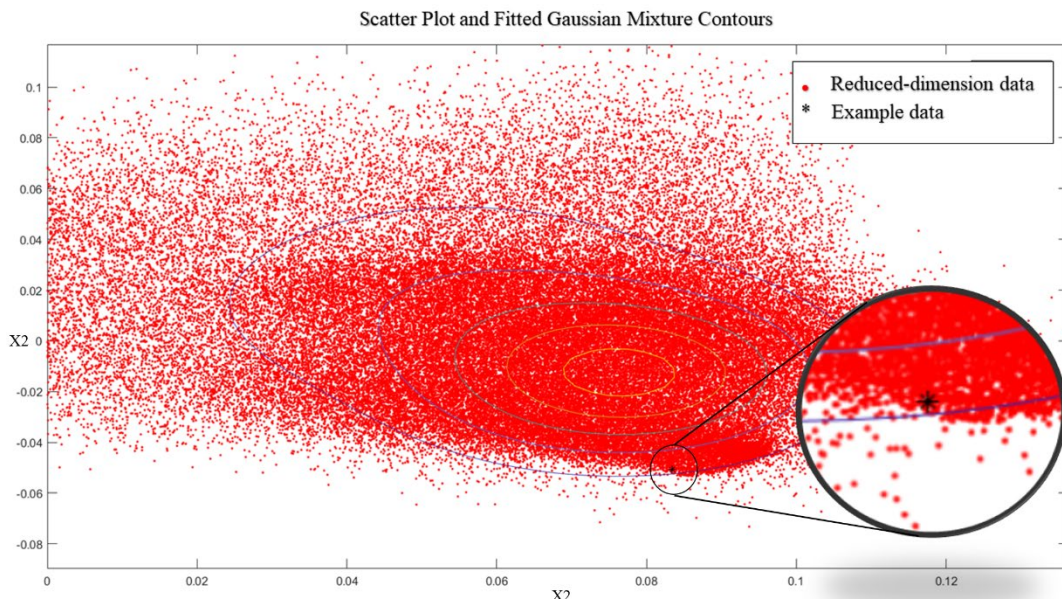


Figure 4.6 The reduced data to 2D along with the fit gaussian model.

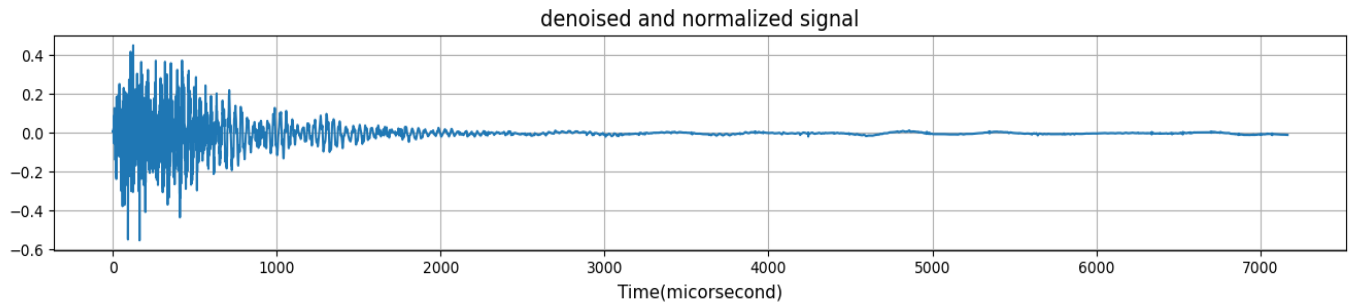


Figure 4.7 Waveform of example data chosen for anomaly detection validation.

#### 4.4.4 VAE

In this section, a DCT was applied to the raw AE signals and then fed to a VAE followed by a DL classification. The main aim of using VAE is to obtain a general feature of the signal that, in turn, could be an input for the DL classifier. Therefore, having the ability to generalize the classifier to be used for different materials without the need for training. A visualization of the model's architecture is presented in Figure 4.8. First, the raw waveform was input to the DCT and the dimension reduced from 7168 to 1000, after that was input to the encoder of VAE, which includes dense layers to encode the data into a latent (hidden) space (100 dimensions), which is much less than 7168 dimensions. This is often called a 'bottleneck' because the encoder performs an efficient compression of the data into this lower-dimensional space. Then decoders "decode" the data to the previous dimension, and finally, by using Inverse DCT, the raw waveform is achieved.

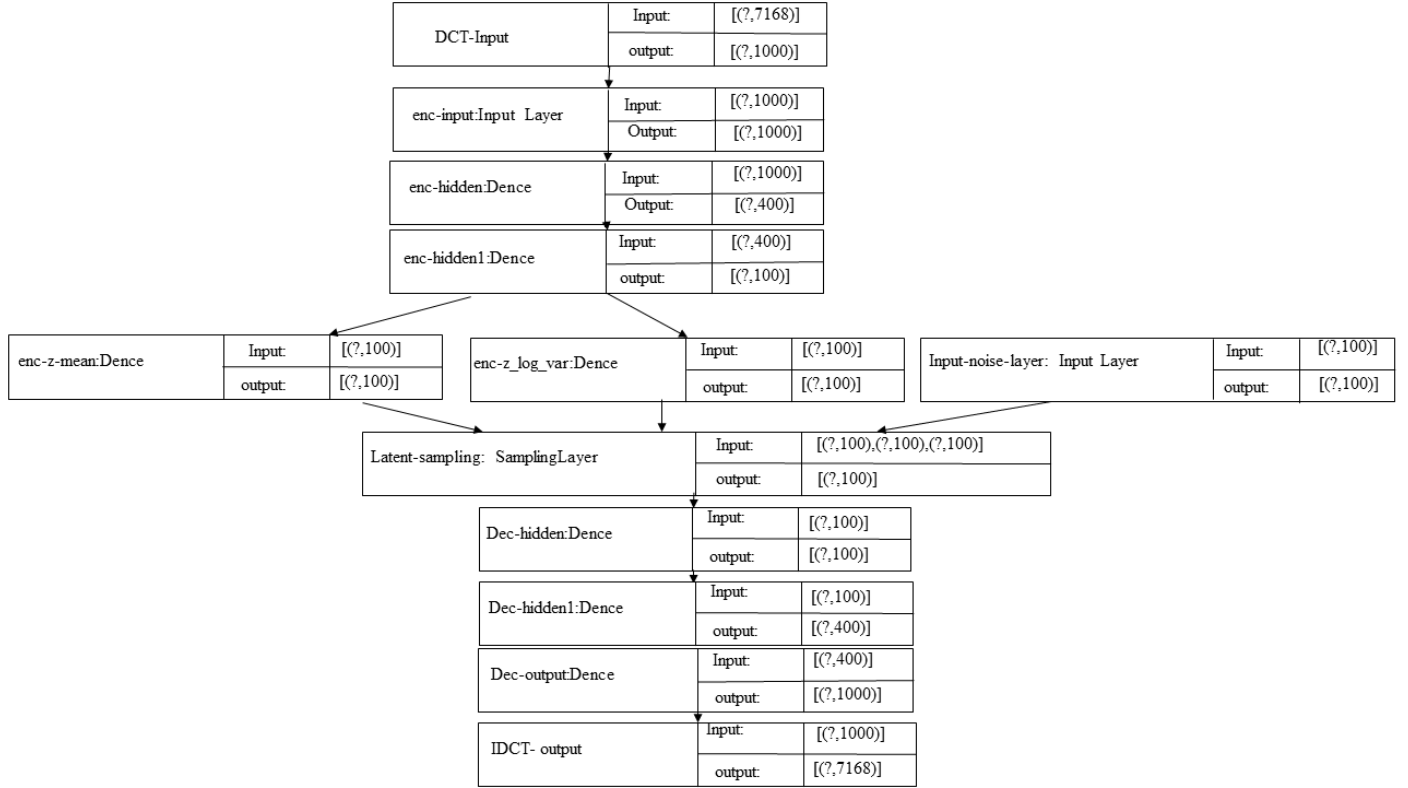


Figure 4.8: The architecture of the combined model.

Figure 4.9 a) shows the variation in loss value for both training and test step errors based on Epoch's number on the H13 data set. The variation in the mean squared error is also provided in Figure 4.9 b). This figure shows a very low mean squared error, and loss values are achieved after 30 epochs. Justifying that the proposed VAE approach can be used for processing the AE signals before classifying them using the DL classifier. Figure 4.10 presents the results of reconstructed signals for a sample. As it is expected, they should be very similar together due to the low loss value. Even with the noise, graph (a) looks remarkably similar to graph (b) in terms of shape, toughs, and peaks.

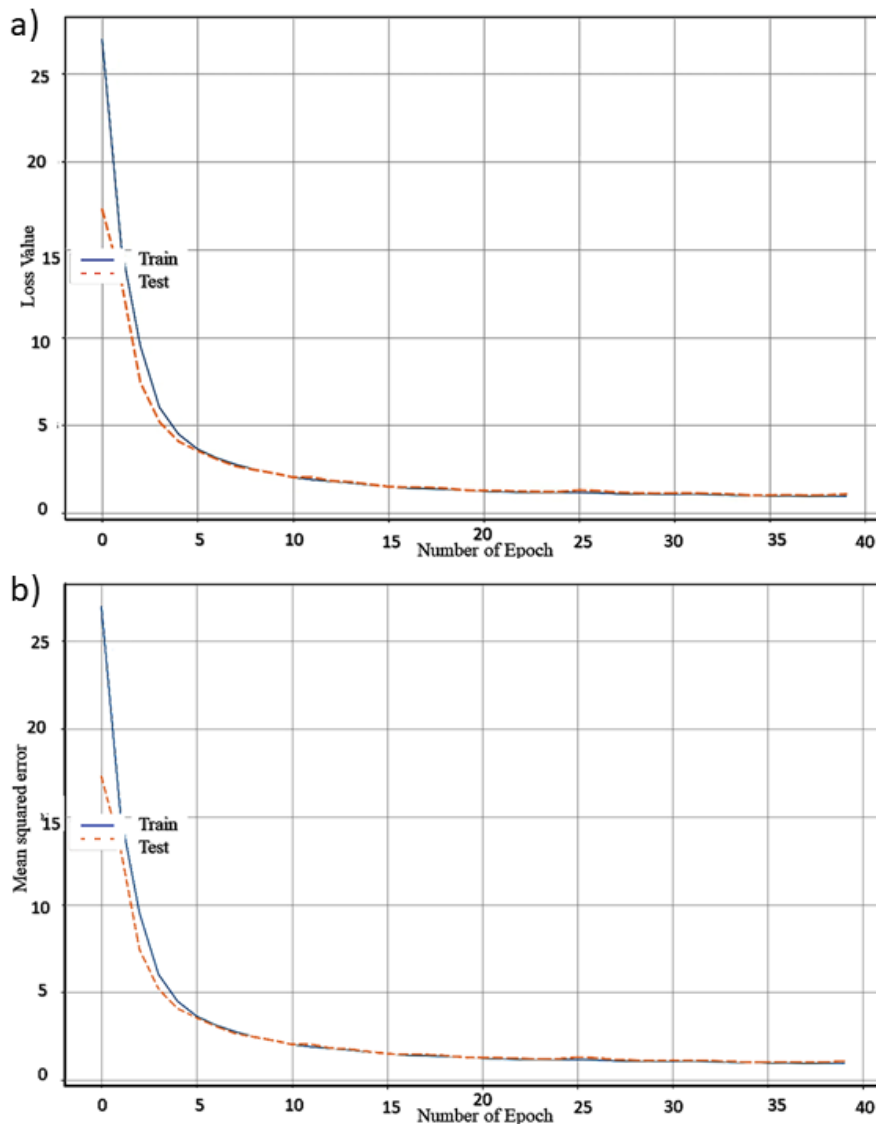


Figure 4.9: a) The loss value and b) the mean squared error versus the number of epochs for the training and test step errors when the learning rate is 0.0020.

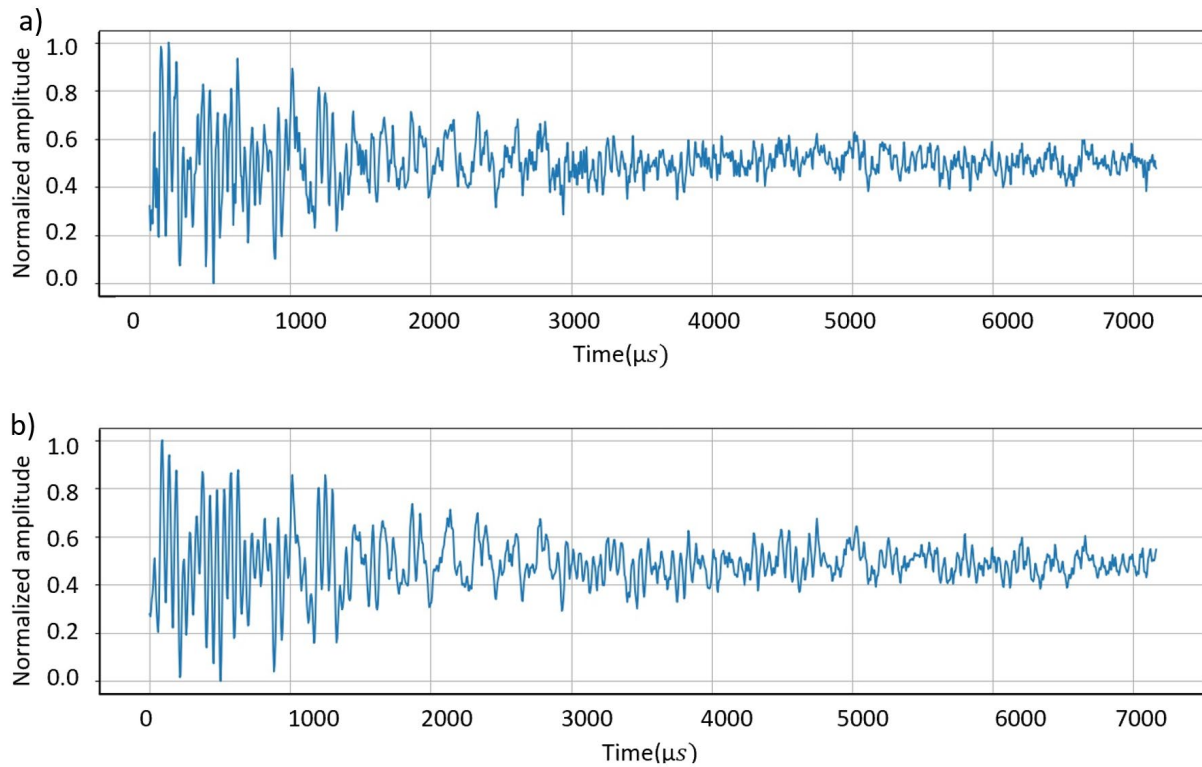


Figure 4.10 The original and reconstructed signal obtained by the proposed VAE structure, a) original signal (encoder input) and b) reconstructed signal (decoder's output).

#### 4.4.5 Generalization of the classifiers

The main idea of generalizing a classifier in this work is developing a DL model that may be used for several materials without training for each material. Two classifiers will be used to test this hypothesis. Both classifiers used the K-means hierarchical method and were trained by the frequency domain H13 AE signal. The collected 316L dataset will be used on these two classifiers to test the generalization concept. Classifier 1 uses the FFT of the 316L AE signals, while classifier 2 will use the VAE approach to the DCT of the AE signal.

The 316L labels are qualitative in nature, which can be categorized as a low, medium, or high-quality level. The quality is defined based on the visual observation of the present cracks and

porosities in the parts' cross-section. Since Classifiers 1 and 2 are trained on H13 datasets, based on the presence of cracks or porosities. Having gone through this training on the H13 dataset, the classifiers are expected to predict more defects in low-quality parts than medium-quality parts and more defects in medium versus high-quality parts when analyzing 316L datasets. This prediction trend would be a useful validation method for the two classifiers.

Table 4-6 and Table 4-7 show the percentage of each test 316L data set divided into low, medium, and high quality, predicted as a defect by classifiers 1 and 2, respectively. Table 4 shows no trend for the no defect signal category as it goes from a high, medium, to low-quality level (61.4%, 69.7%, and 63.6%, respectively). For Porosities, once again, it shows no trend as it goes from high to medium to low quality [21.7%, 28.4%, and 24.1%, respectively]. Lastly, it also exhibits no trend for cracks as it goes from high to medium to low quality [16.9%, 1.9%, and 12.3%, respectively]. In conclusion, there is no evidence from the results presented in Table 4 as to whether classifier 1 predicts more defects in low versus high-quality parts within any category.

Table 4-6: Percentage of defect detection on 316L test dataset by classifier 1.

Reference Signals	High-quality	Medium quality	Low-quality
Minimum defects	61.4%	69.7%	63.6%
Porosity	21.7%	28.4%	24.1%
Cracks	16.9%	1.9%	12.3%

In contrast, Table 5 shows that classifier 2 detects more defects in low-quality parts than other datasets. This table shows a decreasing reference signal trend as the defect-free signal category goes from high to medium to low quality [89.1%, 77.4%, and 63.6%, respectively]. It exhibits an

increasing trend of defect detection as the porosity category goes from high to medium to low quality [8.7%, 8.4%, and 24.1%, respectively]. Lastly, the cracks category has an increasing percentage of defect detection as it goes from high to medium to low-quality parts [2.2%, 14.2%, and 12.3%, respectively].

Table 4-7: Percentage of defect detection on 316L test dataset by classifier 2.

Reference Signals	High-quality	Medium quality	Low-quality
Minimum defects	89.1%	77.4%	63.6%
Porosity	8.7%	8.4%	24.1%
Cracks	2.2%	14.2%	12.3%

By comparing both results, classifier 2 proved to have better accuracy classifying the 316L data without training. It is assumed that frequency-domain data would be better suited as it has a tangible physical meaning, while the VAE hidden layer does not and comes from a numerical neural network layer. While frequency-domain data show good results on the H13 data set when used as an input for machine learning classifiers, the VAE hidden layer is a better input when there is a lack of dataset, such as when new materials are used.

#### **4.5 Conclusion:**

Acoustic emissions monitoring is a non-destructive method that can be implemented to monitor real-time data in additive manufacturing. This study investigates several ML techniques for the purpose of online defect detection during the L-PBF process. First, a hierachal K-Means clustering technique was used to train a DL classifier to detect specific LPBF defects. Results showed a success rate greater than 90%. Second, the application of anomaly detection as an alternative simple and fast machine learning approach was explored by applying a PCA-GMM technique. Finally, a generalized ML model was developed and validated to test data without the need for training. This model uses a VAE hidden layer as generalized input for a deep learning neural network classifier. It was found that the VAE method could classify the 316L dataset without training and detect which parts have more defects according to their quality level, confirming that this method can be successfully employed for other materials as well. The presented study presents the first steps towards optimizing the application of ML techniques for online monitoring of the L-PBF process using AE signature.

#### 4.6 References:

1. Everton, S.K., et al., *Review of in-situ process monitoring and in-situ metrology for metal additive manufacturing*. Materials & Design, 2016. **95**: p. 431-445.
2. Hussein, A., et al., *Advanced lattice support structures for metal additive manufacturing*. Journal of Materials Processing Technology, 2013. **213**(7): p. 1019-1026.
3. Tapia, G. and A. Elwany, *A review on process monitoring and control in metal-based additive manufacturing*. Journal of Manufacturing Science and Engineering, 2014. **136**(6).
4. Frazier, W.E., *Metal additive manufacturing: a review*. Journal of Materials Engineering and performance, 2014. **23**(6): p. 1917-1928.
5. Bhavar, V., et al. *A review on powder bed fusion technology of metal additive manufacturing*. in *4th International conference and exhibition on Additive Manufacturing Technologies-AM-2014*. 2014.
6. Malekipour, E. and H. El-Mounayri, *Common defects and contributing parameters in powder bed fusion AM process and their classification for online monitoring and control: a review*. The International Journal of Advanced Manufacturing Technology, 2018. **95**(1-4): p. 527-550.
7. DebRoy, T., et al., *Additive manufacturing of metallic components – Process, structure and properties*. Progress in Materials Science, 2018. **92**: p. 112-224.
8. Kim, H., Y. Lin, and T.-L.B. Tseng, *A review on quality control in additive manufacturing*. Rapid Prototyping Journal, 2018.
9. Chua, C.K., C.H. Wong, and W.Y. Yeong, *Standards, quality control, and measurement sciences in 3D printing and additive manufacturing*. 2017: Academic Press.
10. Farshidianfar, M.H., A. Khajepour, and A. Gerlich, *Real-time control of microstructure in laser additive manufacturing*. The International Journal of Advanced Manufacturing Technology, 2015. **82**(5-8): p. 1173-1186.
11. Meng, L., et al., *Machine Learning in Additive Manufacturing: A Review*. JOM, 2020: p. 1-15.
12. Yuan, B., et al., *Machine-Learning-Based Monitoring of Laser Powder Bed Fusion*. Advanced Materials Technologies, 2018. **3**(12): p. 1800136.
13. Roberson III, D.M., *Sensor-based online process monitoring in advanced manufacturing*. 2016, Virginia Tech.
14. Taheri, H., et al., *Powder-based additive manufacturing-a review of types of defects, generation mechanisms, detection, property evaluation and metrology*. International Journal of Additive and Subtractive Materials Manufacturing, 2017. **1**(2): p. 172-209.
15. Kruth, J.-P., et al., *Consolidation phenomena in laser and powder-bed based layered manufacturing*. CIRP annals, 2007. **56**(2): p. 730-759.
16. Ye, D., et al., *Characterization of acoustic signals during a direct metal laser sintering process*. 2017, Advances in energy science and equipment engineering II. CRC Press.
17. Narayanan, B.N., et al. *Support vector machine and convolutional neural network based approaches for defect detection in fused filament fabrication*. in *Applications of Machine Learning*. 2019. International Society for Optics and Photonics.
18. Narayanan, B.N., et al. *Automated material identification and segmentation using deep learning for laser powder bed fusion*. in *Applications of Machine Learning 2020*. 2020. International Society for Optics and Photonics.
19. Lu, Q.Y. and C.H. Wong, *Additive manufacturing process monitoring and control by non-destructive testing techniques: challenges and in-process monitoring*. Virtual and physical prototyping, 2018. **13**(2): p. 39-48.
20. Boyes, W., *Instrumentation reference book*. 2009: Butterworth-Heinemann.

21. Wasmer, K., et al. *In situ and real-time monitoring of powder-bed AM by combining acoustic emission and artificial intelligence.* in *International Conference on Additive Manufacturing in Products and Applications.* 2017. Springer.
22. Shevchik, S.A., et al., *Acoustic emission for in situ quality monitoring in additive manufacturing using spectral convolutional neural networks.* Additive Manufacturing, 2018. **21**: p. 598-604.
23. Eschner, N., et al., *Classification of specimen density in Laser Powder Bed Fusion (L-PBF) using in-process structure-borne acoustic process emissions.* Additive Manufacturing, 2020. **34**: p. 101324.
24. Gaja, H. and F. Liou, *Defects monitoring of laser metal deposition using acoustic emission sensor.* The International Journal of Advanced Manufacturing Technology, 2017. **90**(1-4): p. 561-574.
25. Joshi, N., et al., *Acoustic Emission Technology for High Power Microwave Radar Tubes.* 2019: BoD-Books on Demand.
26. Ye, D., et al., *Defect detection in selective laser melting technology by acoustic signals with deep belief networks.* The International Journal of Advanced Manufacturing Technology, 2018. **96**(5): p. 2791-2801.
27. Oran Brigham, E., *The fast Fourier transform and its applications.* UK: Prentice Hall, 1988.
28. Pei, S.-C. and M.-H. Yeh, *The discrete fractional cosine and sine transforms.* IEEE Transactions on Signal Processing, 2001. **49**(6): p. 1198-1207.
29. Shalev-Shwartz, S. and S. Ben-David, *Understanding machine learning: From theory to algorithms.* 2014: Cambridge university press.
30. Okaro, I.A., et al., *Automatic fault detection for laser powder-bed fusion using semi-supervised machine learning.* Additive Manufacturing, 2019. **27**: p. 42-53.
31. Choi, S.W., J.H. Park, and I.-B. Lee, *Process monitoring using a Gaussian mixture model via principal component analysis and discriminant analysis.* Computers & chemical engineering, 2004. **28**(8): p. 1377-1387.
32. Ringnér, M., *What is principal component analysis?* Nature biotechnology, 2008. **26**(3): p. 303-304.
33. Scime, L. and J. Beuth, *Anomaly detection and classification in a laser powder bed additive manufacturing process using a trained computer vision algorithm.* Additive Manufacturing, 2018. **19**: p. 114-126.
34. Altosaar, J., *Tutorial-what is a variational autoencoder.* En ligne, 2019.
35. Srihari, S.N., *Variational Autoencoder Applications.* Center of Excellence for Document Analysis and Recognition (CEDAR).
36. Razvi, S.S., et al. *A review of machine learning applications in additive manufacturing.* in *ASME 2019 international design engineering technical conferences and computers and information in engineering conference.* 2019. American Society of Mechanical Engineers Digital Collection.
37. Li, X., et al., *Quality analysis in metal additive manufacturing with deep learning.* Journal of Intelligent Manufacturing, 2020. **31**(8): p. 2003-2017.
38. Francois, C., *Deep learning with Python.* 2017, Manning Publications Company.
39. Narvan, M., K.S. Al-Rubaie, and M. Elbestawi, *Process-structure-property relationships of AISI H13 tool steel processed with selective laser melting.* Materials, 2019. **12**(14): p. 2284.
40. Mohammadi, M.G. and M. Elbestawi, *Real Time Monitoring in L-PBF Using a Machine Learning Approach.* Procedia Manufacturing, 2020. **51**: p. 725-731.
41. CARPENTER, C.R.H.a.S.H., *ACOUSTIC EMISSION FROM LOW TEMPERATURE PHASE TRANSFORMATIONS IN PLUTONIUM.* Journal of Nuclear Materials 1987. **149**: p. 168-179.
42. Kodinariya, T.M. and P.R. Makwana, *Review on determining number of Cluster in K-Means Clustering.* International Journal, 2013. **1**(6): p. 90-95.

43. Meyer-Baese, A. and V.J. Schmid, *Pattern recognition and signal analysis in medical imaging*. 2014: Elsevier.

## **Chapter 5**

### **Summary and Conclusions**

## 5.1 Summary and conclusive remarks

The monitoring of the L-PBF process was summarized within three significant steps:

First, the AE sensor was set up, the new build-plate, which is compatible with the existing OMNI-SINT L-PBF machine, was designed and produced. Then, the AE sensor was attached under the build-plate, and the AE system parameters were tuned to receive AE signals during each printing step. The process parameters, which were based on previous research on each material, were designed. Finally, each part in a virtual circle was located with the same distance to the AE sensor in mind.

Second, Time-domain AE signals were studied, and it was found that there is an unsteady state in the first 20 layers of printing. The reason behind this initial unsteady state was explained, and references with other researchers showed this idea within thermal and particle size studies.

Third, different machine learning methods were used to investigate the various aspects of AE signals and to correlate them to the specific defects in printed parts. K-Means clustering was used to recognize the pattern of each significant AE event within the printing process, such as AE signals from the recoater or signals from low or high-quality parts. Deep learning was used to classify AE signals from the stainless steel 316L printing process into three classes: high, medium, and low quality. In total, an 85.9% accuracy level was achieved in this classification process. K-means hierarchy was used to separate AE signals based on the defect type. The Deep Learning model classified the results into three different classes; crack, porosity, and reference signals (without cracks or porosities). In total, a 94.56% accuracy level was achieved in this process. An anomaly detection method was used so the model would be high-speed and practical. PCA was

used to reduce the AE signal dimensions to 2D and enable the ability to illustrate data. GMM was fitted to the 2D data and showed the outer circles have the most signals coming from the defects. VAE was used as an alternative feature extraction to present the more general features of AE signals; this was to eliminate the material dependency seen in Deep Learning Classifier. This method was tested on the two material data, SS 316L and Tool steel H13, and showed the potential of the independence of numerical feature extraction by VAE Neural networks.

## 5.2 Strength, limitations, and future work

The effect of online monitoring of the L-PBF process investigated in this thesis helps to guarantee the reliable fabrication of the printed parts. And in case of defects are present, it can inform the system to eliminate the said defect or to stop the process. Acoustic emission enabled individuals to detect micro-cracks in the  $25 \mu\text{m}$  size propagation. Also, it should be mentioned that acoustic emission is one of the low-cost methods available in online monitoring. Different machine learning methods that were used in this thesis help to have a general model for defect detection. Also, using a combination of Machine learning on AE signals shows good potential for monitoring applications in L-PBF.

There are some limitations to obtaining results that would invoke the need for further studies in this area of research. The VAE model proposed in this thesis was tested on two different types of steel; other materials should be investigated as well. In the data collection stage of the project, one AE sensor was used, which can make the monitoring system not reliable enough. For the primary purpose of monitoring, the system will need at least one more AE sensor as a backup in case of

any detaching sensors or other incidents. When having two or more AE sensors, the location of each sensor should be considered as well.

The AE sensor used in this thesis was a wideband frequency sensor, which is very useful for study purposes and laboratory use. However, in the case of industry usage, the narrowband frequency AE sensor will be recommended after acquiring the desired frequency range.

The laser power was the only process parameter changing to reach different qualities in the printed parts. An interesting topic for future studies could be to collect AE data in various process parameters such as changing scan speed or layer thickness. Other outputs for monitoring the L-PBF process include pyrometers, high-speed cameras, infrared cameras, etc. Having a combination of these outputs with AE signals will introduce a reliable monitoring system. In addition, this thesis did not study other AI and machine learning methods that might potentially be good in classification or pattern recognition, such as Support Vector Machine, discriminant analysis, naive Bayesian, k-nearest neighbours, etc. Their potential can be researched in future studies.

### **5.3 Contribution**

This thesis is an essential step in dealing with the online monitoring aspect of the L-PBF process. The findings of this study have contributed to analyzing the received Acoustic emission signals via various machine learning approaches within the time and frequency domain. This thesis also extended the applicability of the acoustic emission for monitoring the L-PBF in more general use cases with various materials. Finally, this thesis suggested multiple machine learning algorithms for pattern recognition and classification with the goal of defect detection, such as detecting cracks and porosities.